Available online at www.sciencedirect.com

SCIENCE DIRECT®

Earth-Science Reviews 73 (2005) 221–243

EARTH-SCIENCE REVIEWS

www.elsevier.com/locate/earscirev

Miocene rapakivi granites in the southern Death Valley region, California, USA

James P. Calzia [a,*], O. Tapani Rämö [b]

[a] U.S. Geological Survey, Menlo Park, CA, USA
[b] Department of Geology, P.O. Box 64, FI-00014 University of Helsinki, Finland

Abstract

Rapakivi granites in the southern Death Valley region, California, include the 12.4-Ma granite of Kingston Peak, the ca. 10.6-Ma Little Chief stock, and the 9.8-Ma Shoshone pluton. All of these granitic rocks are texturally zoned from a porphyritic rim facies, characterized by rapakivi textures and miarolitic cavities, to an equigranular aplite core. These granites crystallized from anhydrous and peraluminous to metaluminous magmas that were more oxidized and less alkalic than type rapakivi granites from southern Finland. Chemical and isotope (Nd–Sr–Pb) data suggest that rapakivi granites of the southern Death Valley region were derived by partial melting of lower crustal rocks (possibly including Mesozoic plutonic component) with some mantle input as well; they were emplaced at shallow crustal levels (4 km) in an actively extending orogen.
Published by Elsevier B.V.

Keywords: rapakivi granite; Death Valley; California; petrology; geochemistry; isotope geology

1. Introduction

In 1891, J.J. Sederholm introduced rapakivi granites to the international geological community in his pioneering paper on Proterozoic granites of southern Finland; since then, southern Finland has been considered the type locality of rapakivi granites. These "type" rapakivi granites are characterized by textures consisting of relatively large crystals of potassium feldspar (K-feldspar) rimmed by plagioclase in a finer grained matrix of quartz and mafic minerals (Fig. 1) and are typically found as discordant plutons intruded into a metamorphic crust; that crust was differentiated from the mantle a few hundred million years earlier (Haapala and Rämö, 1990). Geochemically, the rapakivi granites, crystallized from alkalic, anhydrous, and slightly metaluminous to peraluminous magmas, have high contents of the light rare earth elements (LREE) except Eu, show high Zr, Rb, Ba, Y, F, Fe/Mg, and Ga/Al, low Ca, Mg, P, and Sr, and vary from reduced to oxidized in character (e.g., Anderson and Bender, 1989; Rämö, 1991; Rämö and Haapala, 1995; Frost and Frost, 1997). Rapakivi granites are often associated with bimodal magmatic suites

* Corresponding author. Tel.: +1 650 329 5538; fax: +1 650 329 5130.
E-mail address: jpcalzia@usgs.gov (J.P. Calzia).

0012-8252/$ - see front matter. Published by Elsevier B.V.
doi:10.1016/j.earscirev.2005.07.006

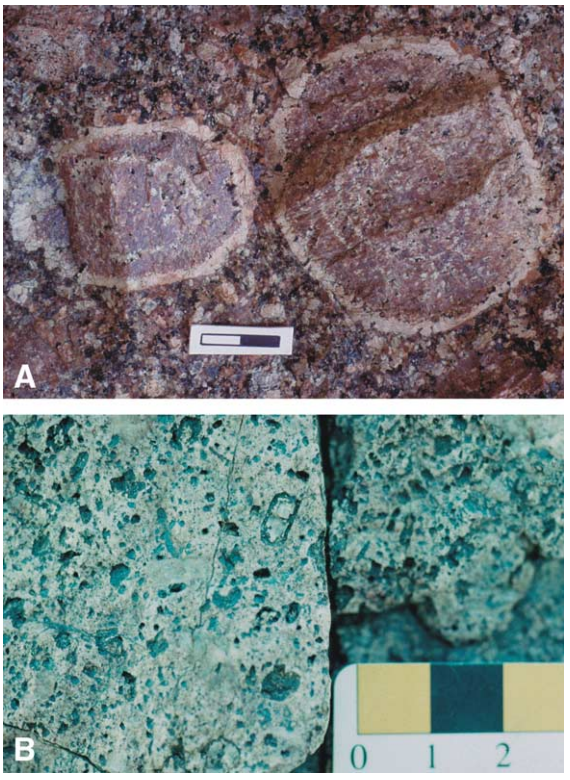

Fig. 1. Photographs showing rapakivi texture in (A) wiborgite (hornblende granite with alkali feldspar megacrysts mantled by sodic plagioclase) from the classic 1.65- to 1.62-Ga Wiborg rapakivi granite batholith of southeastern Finland, and (B) rapakivi porphyry from the 9.76-Ma Shoshone pluton, southern Death Valley region, California. Length of scale bar is 2 cm in (A) and ~3 cm in (B). Photos: O.T. Rämö.

such as anorthosite–mangerite–charnockite–granite complexes as well as spatially and temporally associated mafic dike swarms; this magmatic association has been described in detail from southern Wyoming (Frost et al., 2001), Labrador (Emslie, 1991), Ukraine (Amelin et al., 1994), and Fennoscandia (Rämö, 1991; Neymark et al., 1994; Amelin et al., 1997), and has led many researchers to advocate magmatic underplating as the probable mechanism for generating rapakivi granites (Emslie, 1978; Anderson, 1983; Haapala, 1985; Rämö, 1991). Magmatic underplating may result in partial melting of the lower crust and mixing of lower crust and more mafic melts (Eklund et al., 1994; Salonsaari, 1995).

In the 20th century, rapakivi granites are described from around the world, especially Ukraine, South Greenland, eastern Canada, Brazil, and the United States (see reviews in Rämö and Haapala, 1995; Haapala and Rämö, 1999). In the United States, rapakivi granites are well exposed in areas of pronounced crustal extension and syntectonic magmatism, such as the Colorado River extensional corridor in southernmost Nevada and adjacent Arizona (Volborth, 1973; Falkner et al., 1995; Haapala et al., 2005) as well as the southern Death Valley region in southeastern California (Calzia, 1990). In this paper, we describe three late Cenozoic rapakivi granites from the southern Death Valley region; we compare and contrast their geology, petrography, and geochemistry with Proterozoic rapakivi granites and note the remarkable similarity of these fascinating rocks.

2. Geologic setting

The southern Death Valley region is bounded on the west by the Panamint Range and the south by the Providence and the New York Mountains (Fig. 2). The pre-Cenozoic stratigraphy in this region consists of Early Proterozoic cratonic rocks and Middle Proterozoic to Triassic sedimentary rocks. The cratonic rocks include Early Proterozoic paragneiss, schist, and quartzite intruded by ca. 1700-Ma orthogneiss and 1400-Ma anorogenic granites (Lanphere et al., 1964; Wooden and Miller, 1990; Rämö and Calzia, 1998). The Middle Proterozoic Pahrump Group unconformably overlies the cratonic rocks and consists of approximately 2100 m of conglomerate, sandstone, shale, and carbonate rocks divided into the Crystal Spring Formation, Beck Spring Dolomite, and Kingston Peak Formation (Hewett, 1940); the Crystal Spring Formation is intruded by 1068- and 1087-Ma (Heaman and Grotzinger, 1992) diabase sills. The Pahrump Group is overlain by more than 7500 m of Late Proterozoic to Triassic rocks. The Late Proterozoic and Paleozoic rocks include a basal dolomite overlain by widespread units of quartzite, conglomeratic quartzite, siltstone, shaly siltstone, limestone, and dolomite; the Triassic rocks include metasedimentary and metavolcanic rocks west and south of the Owlshead Mountains.

Most of the miogeoclinal rocks are intruded by Mesozoic and Cenozoic plutons. The Mesozoic plutons vary in composition from granite to gabbro

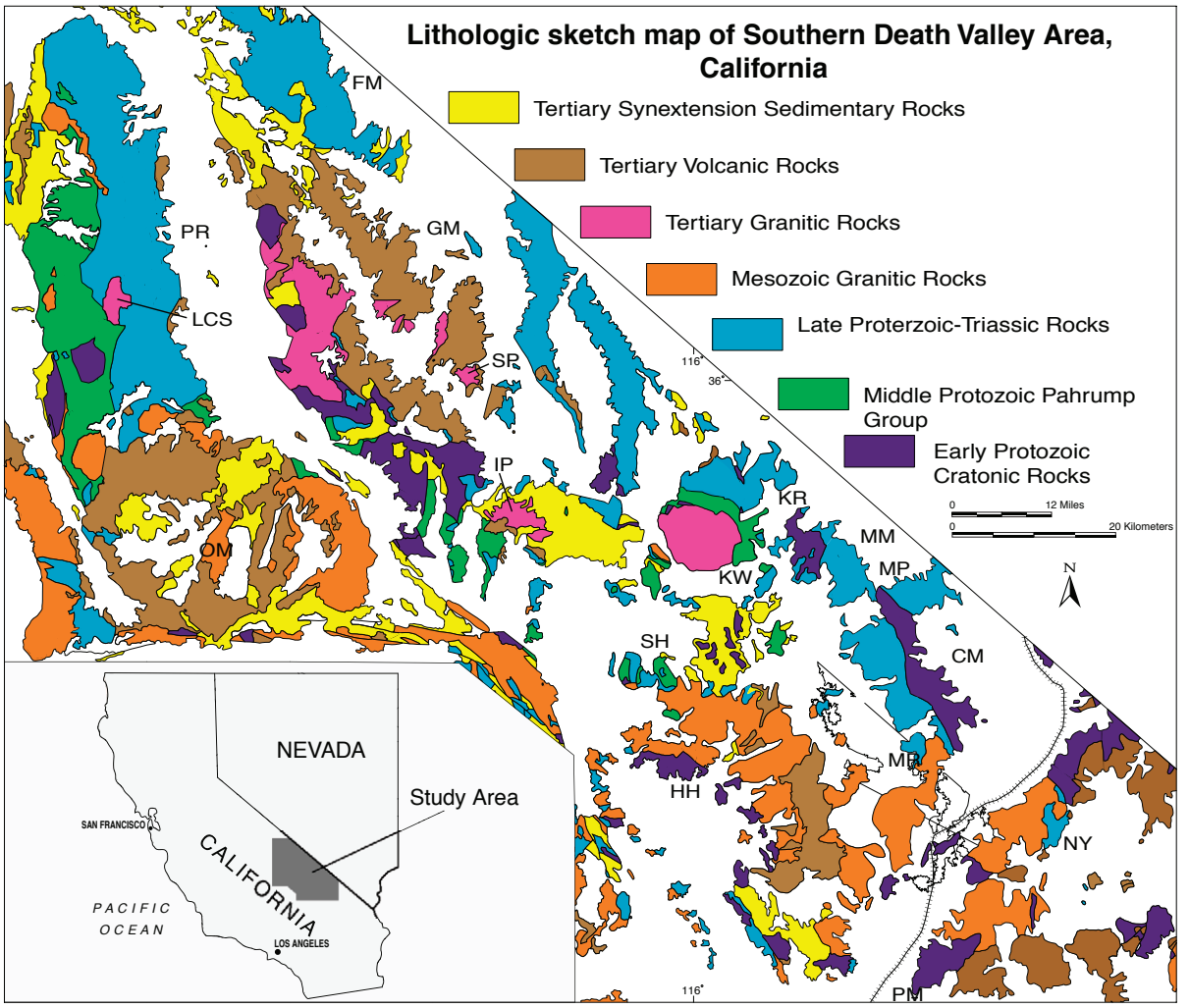

Fig. 2. Index and lithologic sketch map of the southern Death Valley region, California. CM=Clark Mountains, GM=Greenwater Mountains, IP=Ibex Pass, FM=Funeral Mountains, HH=Halloran Hills, KR=Kingston Range, KW=Kingston Wash, LCS=Little Chief stock, MM=Mesquite Mountains, MP=Mesquite Pass, MR=Mescal Range, NY=New York Mountains, OM=Owlshead Mountains, PM=Providence Mountains, PR=Panamint Range, SH=Silurian Hills, SP=Shoshone pluton. Modified from Calzia and Rämö (2000).

(Rämö et al., 2002); Cenozoic plutons vary from granite to quartz monzonite (Calzia and Rämö, 2000). All of these rocks are unconformably overlain by younger Tertiary sedimentary and volcanic rocks and Quaternary alluvial deposits.

The oldest Cenozoic extensional faults in the southern Death Valley region include the Harrisburg and Kingston Range–Halloran Hills fault systems. The Harrisburg fault system along the crest and eastern side of the Panamint Range consists of a basal detachment fault (the Harrisburg fault) and high-angle transfer faults; the Harrisburg fault cuts the Cretaceous Skidoo monzogranite pluton and is cut by late Miocene normal faults (Hodges et al., 1990). Wernicke et al. (1988) reported that the Harrisburg fault is synchronous with fanglomerate and monolithic breccia along the north and northeast side of the range; they tentatively correlated these deposits with the middle Miocene Bat Mountain Formation at the southern end of the Funeral Mountains (Fig. 2). Cemen et al. (1999) redefined the Bat Mountain Formation and concluded that the fanglomerate deposits

at the north end of the Panamint Mountains may be the same age as the basal conglomerate member of their Amargosa Valley Formation; tuff near the base of the conglomerate member yields a K–Ar age of 24.7 ± 0.3 Ma. If this correlation is correct, these data suggest that Cenozoic extension began during the late Oligocene in the Panamint Range.

The Kingston Range–Halloran Hills fault system defines the eastern boundary of the Death Valley extended terrain (Burchfiel et al., 1983) and is divided into northern and southern segments. The Kingston Range detachment fault is well exposed in the northern and eastern Kingston Range to about the latitude of Kingston Wash (Fig. 2). Reconstruction of fault and depositional contacts suggests that maximum horizontal displacement of the hanging wall is about 6 km to the southwest (B.C. Burchfiel, written commun., 1989; Fowler and Calzia, 1999). The Halloran Hills detachment fault is best exposed in Mesquite Pass and the Mescal Range (Fig. 2). Regional geologic relations suggest that rocks in the hanging wall of this detachment fault were transported 5–9 km to the southwest during at least two phases of west-directed sliding (Fowler et al., 1995).

Crosscutting geologic relations bracket the age of crustal extension associated with the Kingston Range–Halloran Hills detachment system. The Kingston Range detachment fault cuts 16.0-Ma (Friedmann, 1996) ash and is cut (Wright, 1968) and deformed (Calzia et al., 1986) by the 12.4-Ma granite of Kingston Peak; 12.5-Ma syntectonic andesite flows are present in the upper plate of the Kingston Range detachment fault (Calzia, 1990). The Halloran Hills detachment fault cuts a 13.4-Ma hypabyssal sill; 13.1-Ma volcanic breccia was deposited on the subsiding hanging wall of this detachment fault (Friedmann et al., 1996). Subhorizontal basalt flows and the undeformed Tecopa lake beds unconformably overlie east-tilted strata related to crustal extension south and west, respectively, of the Kingston Range. The basalt flows yield K–Ar ages of 4.48 Ma (Dohrenwend et al., 1984) and 5.12 Ma (Turrin et al., 1985); the lake beds may be as old as a 7-Ma tuff (Louie et al., 1992). These data indicate that crustal extension in and around the Kingston Range began between 13.4 and 13.1 Ma and stopped by 5 Ma.

3. Rapakivi granites of the southern Death Valley region

Magmatic rocks coeval with Cenozoic extension in the southern Death Valley region include volcanic flows, tuffs, and volcaniclastic deposits as well as granitic plutons, dikes, and sills. Calzia and Finnerty (1984) divided the granitic plutons into two petrogenetic suites based on chemical and textural data. The older suite yields K–Ar ages of 12–14 Ma and consists of alkalic granites characterized by hypabyssal textures, mafic xenoliths, and mantled feldspars. The younger suite yields K–Ar ages of 10–6.5 Ma and consists of calc-alkaline quartz monzonites with medium- to coarse-grained equigranular and porphyritic textures. This paper describes the geology, petrography, and geochemistry of three plutons from the older suite: the granite of Kingston Peak, the Little Chief stock, and the Shoshone pluton. All of these plutons are characterized by rapakivi textures and similar magmatic histories.

3.1. Granite of Kingston Peak

3.1.1. Granite petrography

The granite of Kingston Peak forms an elliptical batholith, 14.6 km long and 10.5 km wide, in the southwest half of the Kingston Range (Fig. 2). This hypabyssal granite intrudes gneiss and the lower member of the Crystal Spring Formation and is divided into (oldest first) feldspar porphyry, quartz porphyry, and aplite facies based on textural variations and intrusive relations. Aplite dikes and quartz veins are common in all three facies; rhyolite porphyry dikes and mafic xenoliths are common only in the feldspar porphyry and quartz porphyry facies. The modes of these rocks are listed in Table 1 and shown in Fig. 3.

The feldspar porphyry facies consists of gray fine- to medium-grained biotite hornblende granite porphyry characterized by seriate feldspar phenocrysts up to 15 mm long, rapakivi textures, and miarolitic cavities. Subhedral to anhedral K-feldspar phenocrysts, 2–4 mm long, are turbid, perthitic, and locally altered to sericite; quartz, plagioclase, and zircon inclusions are common. K-feldspar in the core of rapakivi textures is partially rounded, locally embayed, and bounded by a discontinuous rim of

Table 1
Modal analyses (in volume percent) of Miocene rapakivi granites, southern Death Valley region, CA

Percent phenocrysts and groundmass divided into different minerals and normalized to 100%											
Spl no.	Phenocrysts (<2.0 mm)			Groundmass >(>2.0 mm)							
	Percent phenocrysts	Percent total feldspar		Percent groundmass	Quartz	Plagioclase	K-feldspar	Mafics[a]	Opaque	Vugs	Accessory
		Plagioclase	K-feldspar								
Granite of Kingston Peak											
Feldspar porphyry facies											
4A	35.3	50.4	49.6	64.7	24.6	4.5	68.9	2.0	2.0–3.0		
6A	32.1	68.8	31.2	67.1	37.7	6.7	50.3	5.3	1.0–2.0	0.8	
190.0	19.2	69.8	30.2	80.8	35.4	10.8	49.6	4.2	1.0	0.1	
Quartz porphyry facies											
36.0	6.5	24.6	75.4	93.2	32.8	8.2	51.2	7.8	<1	0.3	
42.0	13.9	60.4	39.6	85.7	21.7	20.1	50.2	8.1	1.0–2.0	0.4	
107.0	39.4	46.3	53.7	60.6	26.8	5.0	61.8	6.5	2.0–3.0		
Aplite facies											
H3	3.2		100.0	96.6	41.6	0.2	56.5	1.7	<1	0.2	
34.0	1.4	57.1	42.9	98.6	34.0	9.0	54.9	2.1	<1	0.3	
Little Chief stock											
Southern facies											
DV74	24.0	50.0	50.0	76.0	31.6	9.9	48.7	7.2	1.3		1.3
Topping A	35.0	14.3	85.7	65.0	46.2	23.1	23.1	3.1*	4.6		
Northern facies											
DV56	43.5	77.0	23.0	56.5	34.5		51.3	9.7	2.7	0.9	
DV128	33.5	9.0	91.0	66.5	37.6	1.5	52.6	6.0	1.5		
DV151	38.0	15.8	84.2	62.0	46.0	1.6	42.7	5.6	1.6	0.8	1.6
Shoshone pluton											
Rim facies											
D2	30.3	76.2	23.8	69.3	22.8	10.7	60.8	3.0*	2.0		
A13	9.9	75.8	24.2	90.1	24.0	10.0	62.5	2.0*	0.6		
Topping D	20.0	65.0	35.0	80.0	28.8	18.8	45.0	6.3*	1.3		
Core facies											
G2	16.3	85.3	14.7	83.8	27.9	7.5	61.0	2.6*	0.5		
E3	25.4	69.3	30.7	74.6	23.1	13.9	57.5	4.0*	0.9		
Aplite facies											
Apl				100.0	12.0	18.0	66.0	3.0*	0.5		

[a] Includes biotite and amphibole.
* biotite only.

quartz mantled by oligoclase; a few mafic minerals occur within the plagioclase mantles. The abundance of mafic minerals in the plagioclase mantle and their absence in the K-feldspar core indicate that these rapakivi textures developed synchronous with or slightly later than crystallization of the mafic minerals. Subhedral to anhedral oligoclase phenocrysts are embayed and fractured; the fractures are filled with opaque oxides.

The fine-grained aplitic groundmass of the feldspar porphyry facies consists of subhedral quartz, K-feldspar, and plagioclase as well as mafic and accessory minerals; graphic granite and granophyric intergrowths are common. Groundmass plagioclase is albite and is more varied in composition than oligoclase phenocrysts. Mafic minerals include biotite and hornblende in nearly equal proportions. Subhedral and anhedral biotite crystals, generally 0.3–0.5 mm and rarely 1 mm across, are pleochroic and poikilitic with apatite, opaque oxides, and zircon inclusions; molar Fe/(Fe+Mg) ratios vary from 0.17 to 0.25. Subhedral to euhedral hornblende crystals are 0.5–0.8 mm long,

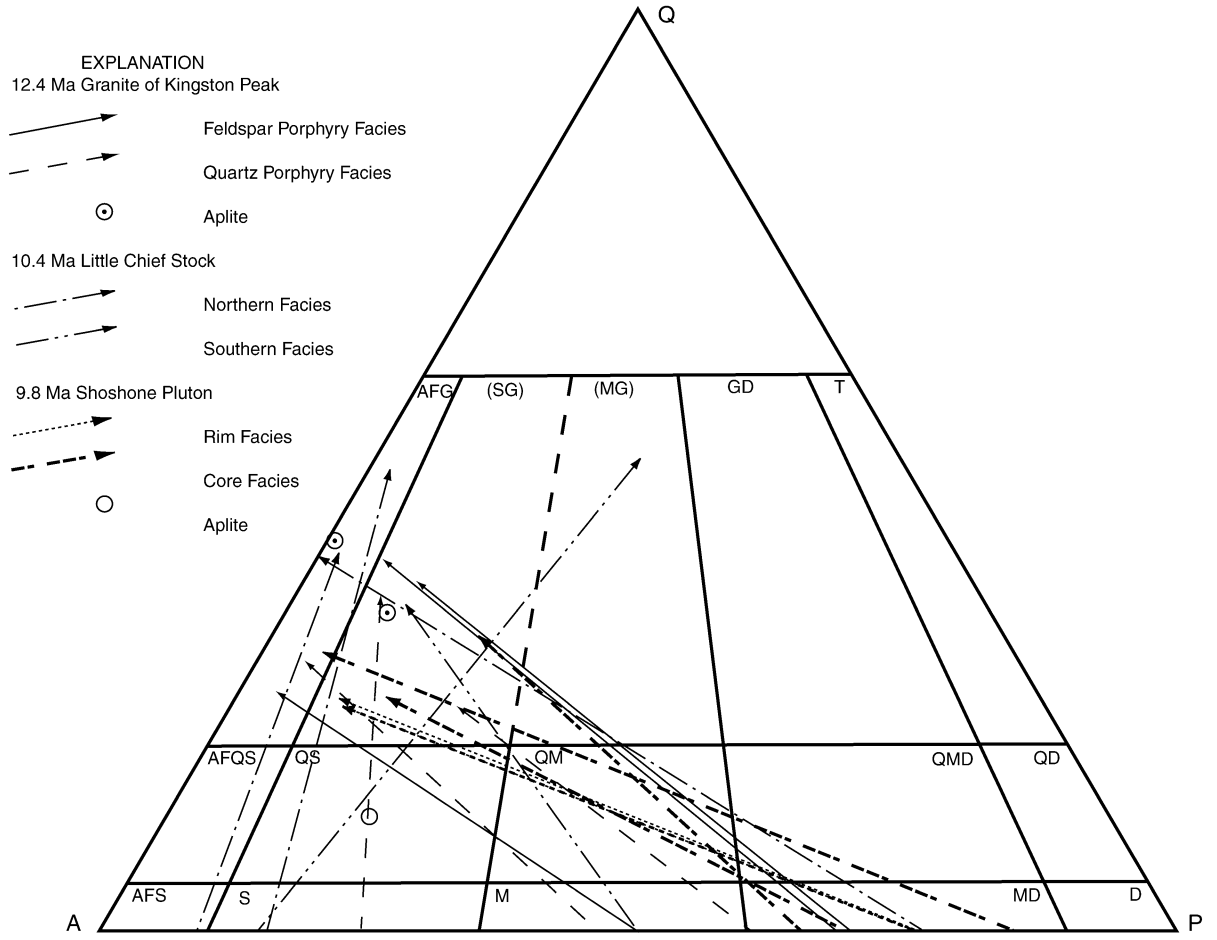

Fig. 3. Modal mineral classification diagram of Miocene rapakivi granites from the southern Death Valley region, California. Arrows represent approximate feldspar tie lines from phenocrysts to groundmass compositions. Q=quartz, A=alkali feldspar, P=plagioclase; Q+A+P=100%. Field boundaries and nomenclature from Streckeisen (1973).

usually altered to chlorite and opaque oxides, and often covered by a reddish brown opaque dust; molar Mg/(Mg+Fe) ratios from hornblende vary from 0.71 to 0.73. Clots of biotite, titanite, and opaque oxides form pseudomorphs after amphibole; these clots probably represent hornblende that has reacted with the melt during crystallization. Accessory minerals include anhedral zircon inclusions in K-feldspar, plagioclase, and biotite, subhedral to euhedral apatite that forms blunt equant crystals 0.2–0.3 (locally up to 0.5) mm long, and subhedral titanite with opaque oxides, apatite, and zircon inclusions. Euhedral and anhedral opaque oxides are 0.2–0.8 mm across and contain apatite inclusions.

The quartz porphyry facies consists of pale gray to white fine- to medium-grained granite porphyry characterized by anhedral (subrounded) quartz phenocrysts, up to 2 or 3 mm across, and seriate feldspar phenocrysts up to 12 mm long; perthite, graphic granite, granophyric intergrowths, and rapakivi textures are common. The quartz phenocrysts locally contain subhedral K-feldspar inclusions. Subhedral to anhedral K-feldspar phenocrysts are generally 1–2 mm long (maximum 5–8 mm) and contain many inclusions of quartz and plagioclase. K-feldspar in the core of rapakivi textures is rounded and bounded by a discontinuous quartz rim mantled by plagioclase; antirapakivi textures are rare but are more common in this

facies than in the feldspar porphyry facies. Anhedral to subhedral oligoclase phenocrysts are generally 1–4 mm long and rarely up to 12 mm long. These phenocrysts are poikilitic with abundant anhedral quartz, K-feldspar, and mafic inclusions.

The groundmass of the quartz porphyry facies is aplitic and consists of anhedral (rarely subhedral) very fine-grained quartz, perthitic K-feldspar, and plagioclase; miarolitic cavities are common and are often filled by secondary quartz. Biotite occurs as individual anhedral and subhedral crystals, 0.5–1.0 mm across, or in clots, up to 3 mm long, with opaque oxides. Biotite crystals are pleochroic and poikilitic with euhedral apatite and zircon inclusions; Fe/(Fe+Mg) varies from 0.26 to 0.3. Hornblende is absent although most of the clots of biotite and opaque oxides (locally with zircon and feldspar) form pseudomorphs after amphibole. Accessory minerals include large (0.4–0.6 mm) euhedral opaque oxides, subhedral to euhedral apatite crystals up to 0.2 mm long, and anhedral zircon; titanite is rare or absent. The quartz porphyry facies contains about as much opaque oxides as does the feldspar porphyry facies; the abundance of opaque oxides decreases, however, toward contacts with the older rocks. Smaller (=0.1 mm) opaque oxide crystals and zircon occur as inclusions in biotite.

The aplite facies is generally fine-grained and equigranular but does contain a few (≤3%) K-feldspar phenocrysts; miarolitic cavities, graphic granite, and granophyric intergrowths are common. Anhedral to subhedral quartz crystals are generally 0.2–0.3 mm across; K-feldspar phenocrysts, up to 2 mm long, are subhedral and perthitic. Plagioclase occurs as euhedral crystals of albite and oligoclase in the groundmass and as anhedral inclusions of calcic-rich oligoclase in the K-feldspar phenocrysts. Subhedral to euhedral biotite crystals are poikilitic with apatite inclusions; amphibole is absent. Accessory minerals include subhedral apatite, characterized by rounded terminations, and rare zircon. Titanite is nearly absent; a single crystal was observed in one aplite plug in the feldspar porphyry facies. The aplite facies contains less than one percent subhedral to euhedral opaque oxides uniformly distributed throughout the rock.

3.1.2. Mafic xenoliths

Mafic xenoliths are found as rounded to irregular-shaped clots (up to 10 mm across) or teardrop-shaped inclusions (up to several centimeters long) in the feldspar porphyry and quartz porphyry facies. The xenoliths are widely scattered throughout the batholith but are most common near the contact between these two facies. Dark, teardrop-shaped vesicular mafic xenoliths form sharp contacts with the feldspar porphyry facies; thin discontinuous gray zones around the margin of a few xenoliths are caused by small apophyses of the granite in the xenolith.

The mafic xenoliths consist mainly of fine-grained subhedral andesine, hypersthene mostly altered to chlorite, and abundant opaque oxides; green hornblende, up to 6 mm long, is common. Spherulitic biotite forms a reaction rim around an unidentified mafic mineral that is completely altered to chlorite or actinolite; the shape of the biotite reaction rim suggests that the original mineral was amphibole. A few embayed and skeletal crystal clots have clinopyroxene habit but are completely altered to chlorite, biotite, and opaque oxides; their original composition could not be identified.

The feldspar porphyry facies adjacent to the mafic xenoliths is generally finer grained and contains less plagioclase that is more sodic than normal for this rock; green hornblende, locally with blue pleochroism, is common. The change in pleochroism indicates that the hornblende is more sodic than other hornblendes in this facies. Rare orthopyroxene crystals in the granite are completely surrounded by opaque oxides and are altered to talc or actinolite. The abundance and texture of the orthopyroxene crystals suggest that they are xenocrysts not in equilibrium with the adjacent melt during crystallization.

3.1.3. Dikes and veins

Rhyolite porphyry and aplite dikes as well as quartz veins are common in and adjacent to the granite of Kingston Peak. The rhyolite porphyry dikes cut all but the aplite facies of the granite of Kingston Peak and are cut by aplite dikes. Quartz veins fill joints and faults that crosscut the dikes and are the youngest rocks coeval with the granite of Kingston Peak.

Gray, white, and purple biotite rhyolite porphyry dikes consist of quartz and K-feldspar phenocrysts in an aphanitic groundmass; euhedral to subhedral oligoclase and albite phenocrysts are rare. The groundmass consists of very fine-grained subhedral to anhedral quartz and turbid K-feldspar. Subhedral

hornblende crystals with tan to green pleochroism are rare and are restricted to the coarser-grained cores of the larger dikes. Most hornblende crystals are replaced by clots of subhedral brown biotite altered to chlorite or actinolite, opaque oxides, and red brown opaque stain. Accessory minerals include fine-grained subhedral to euhedral opaque oxides, very fine-grained anhedral zircon, and equant or elongate apatite crystals up to 0.2 mm long.

Fine-grained equigranular aplite dikes consist of subhedral to anhedral quartz, subhedral perthitic K-feldspar, albite, and less than one percent opaque oxides. Subhedral biotite crystals with apatite inclusions are generally less abundant than opaque oxides but locally constitute 1% to 3% of the rock; amphibole(?) completely altered to chlorite is rare.

White quartz veins are most common in the eastern half of the batholith. Although the veins are generally massive, color bands and vesicles are common; the vesicles are locally filled with amethyst. Locally, the vesicles are so common that the veins develop a "honeycomb" or crude stockwork texture on weathered surfaces; these stockwork veins contain anomalous concentrations of lead and barium but no sulfide or oxide minerals (Calzia et al., 1986). The "honeycomb" texture is caused by erosion and leaching of soluble inclusions (probably carbonate material).

3.1.4. Age

The age of the granite of Kingston Peak was determined by conventional K–Ar and $^{40}Ar/^{39}Ar$ methods (Calzia, 1990). Biotite and hornblende from the feldspar porphyry facies yield concordant K–Ar ages of 12.1 ± 0.9 and 12.4 ± 0.3 Ma, respectively. Incremental heating of hornblende from the same sample yields a plateau age of 12.42 ± 0.04 Ma for more than 95% of the ^{39}Ar released during the experiment, and a recombined total fusion age of 12.36 ± 0.18 Ma. The concordant K–Ar and $^{40}Ar/^{39}Ar$ ages indicate that the granite of Kingston Peak is middle Miocene.

3.1.5. Granite of Ibex Pass

The fine- to medium-grained granite of Ibex Pass in the Sperry Hills (Fig. 2) is characterized by rapakivi textures and is modally, chemically, and isotopically equivalent to the 12.4-Ma granite of Kingston Peak (Calzia et al., 1991); biotite from the granite of Ibex Pass yields a K–Ar age of 12.6 ± 0.3 Ma (J.P. Calzia, unpublished data). Although Burchfiel et al. (1985) suggested that granitic rocks in the Sperry Hills once rested on the granite of Kingston Peak, L.A. Wright (written commun., 1993) and McMackin (1997) proposed that the granite of Ibex Pass is autochthonous bedrock. The granite of Ibex Pass has no exposed intrusive contacts; it tectonically overlies miogeoclinal rocks south of Tecopa Peak, and is tectonically interleaved with late Miocene China Ranch beds in the Sperry Hills. Isostatic gravity data indicate that this granite forms a tabular body approximately one km thick and is rootless (Calzia et al., 1991). These geologic and geophysical data, combined with chemical, isotopic, and geochronological observations, support the Burchfiel et al. hypothesis, as refined by Topping (1993) and Holm et al. (1994), and suggest that the granite of Ibex Pass is a large landslide deposit derived from the granite of Kingston Peak.

Disaggregated hypersthene occurs in vesicular mafic xenoliths in the granite of Ibex Pass. Hypersthene is surrounded by, and isolated from, the xenolith host by an assemblage of quartz, feldspar, biotite, titanite, and zircon characterized by a medium-grained granitic texture. Modal and textural data suggest that these granitic assemblages represent blebs of granitic melt that invaded the xenolith host; the abundance and shape of these blebs, as well as their close spatial association with disaggregated hypersthene, suggest that the granitic melt filled vesicles and reacted with hypersthene in the mafic xenolith. These observations, combined with the abundance of orthopyroxene xenocrysts in the granite of Kingston Peak, indicate that some type of magmatic and chemical interaction occurred between Cenozoic granitic and mafic melts in the southern Death Valley region.

3.2. Little Chief stock

3.2.1. Granite petrography

The Little Chief stock is a dome-shaped hypabyssal stock along the crest of the Panamint Range south of Telescope Peak (Fig. 2). This stock, 28 km^2 in outcrop, intrudes the Pahrump Group as well as the oldest miogeoclinal rocks, with sharp discordant contacts; a chill zone approximately 0.3 m wide is common between the stock and the country rocks (Albee

et al., 1981). Regional cross sections suggest that the Little Chief stock has a flat floor at the contact between gneiss and carbonate rocks in the Pahrump Group (McDowell, 1967).

The Little Chief stock is divided into southern and northern facies (McDowell, 1967). The contact between facies is sharp; apophyses within the chill zone indicate the southern facies is intruded by the northern facies. Inclusions of an earlier magmatic phase are common in both facies.

The southern facies consists of medium gray hornblende–biotite granite with plagioclase and sanidine phenocrysts, 2–5 mm across, in a very fine-grained (0.2–0.5 mm) groundmass of K-feldspar, quartz, and plagioclase; megacrysts of K-feldspar and plagioclase, up to 15 mm across, are present but rare. Plagioclase phenocrysts are characterized by embayed calcic cores with sodic plagioclase rims; compositions vary from andesine to oligoclase from core to rim, respectively. The rims are characterized by one to three compositional reversals and locally yield very sodic compositions. Subhedral sanidine phenocrysts are usually embayed and bounded by rims of cloudy or mottled oligoclase; quartz blebs along the core/rim boundary are common. The groundmass consists of quartz, sanidine, plagioclase, and less than seven percent mafic minerals. Groundmass sanidine forms equant crystals, locally with zoned plagioclase cores. Plagioclase in the groundmass occurs as glomeroporphyritic aggregates, up to 10 mm across, associated with hornblende and biotite.

The northern facies is divided into exterior and interior phases; contact relations indicate that the exterior phase was intruded by the interior phase (McDowell, 1967). The exterior phase consists of pinkish gray biotite–hornblende granite with plagioclase and sanidine phenocrysts up to 7 mm across; the interior phase is similar and consists of white to very light gray hornblende–biotite granite with phenocrysts up to 10 mm across. Euhedral to subhedral plagioclase phenocrysts consist of embayed labradorite cores with oligoclase rims. Albite twins are common in the cores of these phenocrysts; the rims are zoned but not twinned. Euhedral to subhedral sanidine phenocrysts have partially embayed cores and oligoclase rims 0.5–1 mm wide; inclusions of euhedral plagioclase with albite twins are common in the core of sanidine phenocrysts. The inclusions occur as laths aligned with the long dimension of the sanidine host, as disoriented inclusions near the outer edge of sanidine phenocrysts, or as patch perthite; graphic granite is common. The groundmass of the exterior and interior phases consists of quartz, sanidine, plagioclase, and $<10\%$ mafic minerals 1–6 mm long; megacrysts of plagioclase aggregates and sanidine up to 20 mm across are common. Vugs up to 5 mm in diameter as well as pegmatite and aplite dikes are common in the northeast part of the northern facies; the vugs constitute less than one percent of the rock.

A contact facies surrounds the northern facies as well as the east side of the southern facies and consists of anhedral sanidine and plagioclase phenocrysts in a fine grained groundmass; vermicular to graphic granite textures are common in the groundmass of the contact facies. Sanidine phenocrysts are characterized by lamellar perthite; plagioclase phenocrysts are complexly zoned with andesine cores and oligoclase rims; the outer edge of the rims includes a thin compositional reversal to andesine.

Mafic and accessory minerals, including hornblende, biotite, titanite, magnetite, and apatite, are common in all facies of the Little Chief stock. Hornblende generally forms euhedral prisms, 0.2–5 mm long; $Fe/(Fe+Mg+Mn)$ is approximately 0.5. The core of hornblende crystals is often skeletal and replaced by biotite, quartz, and K-feldspar. Calcium- and magnesium-rich augite is present but rare in the core of several hornblende crystals in the southern facies; reaction rims of biotite and diopside around hornblende are common in the contact facies. Euhedral to anhedral biotite occurs as scattered plates up to 1 mm across or in clots of hornblende, magnetite, and plagioclase in the groundmass; the biotite plates yield lower $Mg/(Mg+Fe)$ than groundmass biotite. Biotite pseudomorphs after pyroxene are common throughout the stock. Titanite crystals, 0.1–0.6 mm long, are euhedral but skeletal. Magnetite is anhedral and less than 1 mm across. Apatite occurs as a replacement product after Na-plagioclase and K-feldspar.

3.2.2. Magmatic inclusions

Round inclusions of an earlier magmatic phase are concentrated in an east–west zone near the contact between the southern and northern facies. The inclusions consist of green very fine-grained igneous rock with sanidine phenocrysts in a groundmass of quartz

and plagioclase. The sanidine phenocrysts are rimmed by cloudy plagioclase with quartz blebs; plagioclase laths in the groundmass are 0.2–1 mm long and rimmed by K-feldspar. The igneous inclusions consist of 20–25% mafic and accessory minerals including hornblende, biotite, magnetite, titanite, apatite, and secondary chlorite; hornblende is locally rimmed by diopside. The inclusions include rapakivi and anti-rapakivi textures and are not flow banded. Some inclusions include euhedral plagioclase phenocrysts with numerous quartz blebs and albite twinning.

3.2.3. Dikes

Felsic dikes and sills that are pre- and synmagmatic with the Little Chief stock are divided into two dike swarms (McDowell, 1967). North-trending porphyritic rhyolite dikes that extend from the northeast corner of the stock are truncated by the northern facies and are older than the Little Chief stock. Many of these dikes trend into breccia that consists of angular fragments of country rocks in a matrix of dike rock. A southern dike swarm consists of a vertical 100-m-thick dike that divides into numerous subparallel dikes. This dike swarm follows pre-existing faults and is 100–300 m wide approximately 0.5 km from the stock.

A dike sheath injected between the Little Chief stock and the country rocks consists of very fine-grained aplite characterized by spherulites and gray laminations; inclusions of dolomite, approximately 30 m long, are stoped into the dike sheath. The dike sheath is older than the southern facies, younger than the northern dike swarm, and is synmagmatic with the northern facies of the Little Chief stock (McDowell, 1967).

3.2.4. Age

K-feldspar from a monzonite boulder at the mouth of Hanaupah Canyon yields a conventional K–Ar age of 12.5 ± 1.3 Ma (Stern et al., 1966). Hodges et al. (1990) reported a three-point Rb–Sr isochron of 10.6 ± 0.2 Ma using plagioclase, biotite, and hornblende. Topping (1993) reported a zircon fission-track age of 11.2 ± 0.5 Ma for the southern facies and 9.8 ± 0.5 Ma for the northern facies. Although discordant, the isotopic data suggest that the Little Chief stock is middle Miocene and may be as old as 12.5 Ma.

3.3. Shoshone pluton

3.3.1. Granite petrography

The Shoshone pluton is the youngest intrusive rock in the southern Greenwater Mountains (Fig. 2). This elliptical pluton, 3 km wide and 4 km long, is tilted to the east and has no exposed intrusive contacts; it is unconformably overlain by Miocene volcanic rocks.

The Shoshone pluton consists of gray porphyritic quartz monzonite with phenocrysts of plagioclase and K-feldspar in pink groundmass. The pluton is texturally zoned into rim, core, and aplite facies. The rim facies is intruded by the core facies; both are characterized by miarolitic cavities and rapakivi textures.

The rim and core facies consist of phenocrysts of plagioclase, microcline, quartz, and biotite as well as rare pseudomorphs of brown chlorite, hematite, and calcite after amphibole. Euhedral to subhedral oligoclase phenocrysts are 0.2–1.0 cm across and are zoned and sericitized. Microcline occurs as ovoid phenocrysts or as micrographic intergrowths with quartz; the ovoid phenocrysts are slightly perthitic and rimmed by oligoclase (Fig. 1B). The interface between microcline and oligoclase is uneven to serrate; the oligoclase rim is slightly more Ab-rich than coexisting plagioclase phenocrysts. Subhedral quartz phenocrysts are strongly embayed. Euhedral biotite phenocrysts are rimmed by aggregates of magnetite, zircon, and ilmenite needles; $FeO^*/(FeO^* + MgO)$ of biotite varies from 0.48 to 0.5. Euhedral to anhedral magnetite occurs as reaction rims around dark reddish-brown biotite phenocrysts; the magnetite is oxidized to hematite (locally limonite), Mn-rich ilmenite, and pseudobrookite.

The rim and core facies are differentiated by aphanitic and granophyric groundmass, respectively (Almashoor, 1980). The aphanitic groundmass consists of an equigranular aggregate of microcline, quartz, and plagioclase; the granophyric groundmass is characterized by resorbed quartz microphenocrysts, 1.5 mm in diameter, that include cuneiform, vermicular, and radiating textures. The groundmass of each facies contains less than five percent biotite and magnetite; apatite inclusions and red brown rutile needles are common in groundmass biotite.

The white fine-grained aplite facies is equigranular and consists of anhedral plagioclase and granophyric intergrowths of quartz and K-feldspar. Although the contact with the core facies is poorly exposed, Alma-

shoor (1980) concluded that the aplite facies is a late differentiate of the core facies.

3.3.2. Xenoliths, inclusions, and dikes

The Shoshone pluton includes numerous green xenoliths as well as green and gray inclusions and is cut by several generations of dikes. The green xenoliths are igneous in origin, felsic to intermediate in composition, and are rounded, up to 15 m in diameter, or elongated north–south. Dark green quartz diorite inclusions consist of fine- to coarse-grained hornblende in a groundmass of white feldspar; the randomly oriented hornblende crystals are 1–1.5 cm long and are characterized by acicular to lath-shaped textures. Gray felsic inclusions consist of 20–25% plagioclase, rare K-feldspar, one to two percent hornblende, and are characterized by granophyric textures and mafic inclusions.

Latite, andesite, and lamprophyre dikes cut the Shoshone pluton. Pink fine-grained quartz latite dikes consist of plagioclase and K-feldspar phenocrysts, up to 5 mm long, in a microcrystalline groundmass. These dikes are 1.5–5 m wide and locally emplaced along faults that are synmagmatic with the Shoshone pluton. Green andesite dikes and plugs consist of plagioclase, augite, hypersthene, and magnetite; plagioclase crystals are characterized by concentric compositional zoning. One andesite dike cuts a latite dike and co-mingles with the quartz monzonite. Andesite plugs are elliptical and as much as 25 m long. Dark gray to greenish gray porphyritic lamprophyric dikes consist of dark green hornblende and rare biotite phenocrysts in a holocrystalline groundmass of hornblende, andesine, and minor biotite.

3.3.3. Age

The Shoshone pluton is disconformably overlain by 7.5- to 8.5-Ma (Wright et al., 1991) dacite and rhyolitic flows and tuffs of the Shoshone Volcanics; biotite from the rim facies yields a $^{40}Ar/^{39}Ar$ total fusion age of 9.76 ± 0.25 Ma (Holm et al., 1992). These data suggest that the Shoshone pluton is late Miocene.

4. Geochemistry

The chemical compositions of rapakivi granite samples from the southern Death Valley region are listed in Table 2 and shown on Figs. 4 and 5. Samples from these granites span a relatively large range in SiO_2 (69.8 to 77.6 wt.%), straddle the peraluminous–metaluminous boundary (Fig. 4A), are moderately enriched in Fe relative to Mg (FeO*/[FeO*+MgO] varies from 0.75 to 0.95; Fig. 4B), have high alkali metal and intermediate high field strength element (HFSE) contents (Fig. 4C), and mostly plot in the within-plate field on Nb vs. Y tectonomagmatic discrimination diagrams (Fig. 4D). The Shoshone pluton is less enriched in Fe relative to Mg (Fig. 4B) and has lower contents of HSFE than the granite of Kingston Peak, granite of Ibex Pass, and Little Chief stock. Thus the Shoshone pluton is less like typical A-type (Fig. 4C) and within-plate (Fig. 4D) granites than other rapakivi granites in the southern Death Valley region.

Chemical analyses of the ca. 1.6 Ga rapakivi granites of Finland and 1.88 Ga anorogenic granites from the Amazon craton are also shown on Fig. 4. Rapakivi granites in the southern Death Valley region are similar to the Finnish rapakivi granites in terms of aluminum saturation and within-plate geochemical character (Fig. 4A and D), but are, in general, not as strongly enriched in Fe relative to Mg and HFSE (Fig. 4B and C). These data indicate that rapakivi granites in the southern Death Valley region are more oxidized than the "type" rapakivi granites (cf. Frost and Frost, 1997); they more nearly resemble the more oxidized anorogenic granites of the Amazon craton (Fig. 4B; Dall'Agnol et al., 1999).

The rare earth element (REE) content of rapakivi granites in the southern Death Valley region is shown in chondrite-normalized diagrams in Fig. 5. The overall patterns of these three plutons are similar and show a slightly less pronounced enrichment in heavy REE relative to rapakivi granites from Finland (Fig. 5A–C). Relative enrichment in REE contents may be caused by a lower degree of partial melting of the source rocks of the Death Valley granites.

The initial Nd, Sr, and Pb isotope compositions of the Miocene rapakivi-type granites in the southern Death Valley region are listed in Table 3 and shown in Figs. 6 and 7. Fig. 6 shows the initial Nd and Sr isotope compositions of these rapakivi granites compared to those of Mesozoic granitoids from the Sierra Nevada and Peninsular Ranges batholiths, Cretaceous granitoids of the Mojave Desert, and Cretaceous batholiths of the southern Death Valley region. The rapa-

Table 2
Geochemistry of Miocene rapakivi granites, southern Death Valley region, California

Area	Kingston Range													Sperry Hills		Panamint Mtns			Greenwater Mtns		
Name	Granite of Kingston Peak								Mafic xenolith	Dikes			Syenite, Peak 4611	Granite of Ibex Pass		Little Chief stock			Shoshone pluton		
Description	Feldspar porphyry facies			Quartz porphyry facies			Aplite facies			Mafic	Rhy. porp.	Aplite				Southern phase					
Sample no.	4A	6A	190	42	36	107	H3	34	170	164	43	166	47	52	276	LCS	3B	Topping A	10	126	Topping D
Major element geochemistry (wt.%)																					
SiO_2	72.90	71.10	71.80	69.70	71.90	71.40	77.60	74.40	54.30	60.00	70.70	69.00	68.70	72.60	72.20	69.80	67.98	74.64	70.50	70.80	71.16
TiO_2	0.28	0.35	0.33	0.40	0.33	0.36	0.11	0.14	1.15	0.73	0.42	0.46	0.38	0.34	0.40	0.42	0.43	0.21	0.34	0.36	0.34
Al_2O_3	13.60	14.10	14.20	15.00	13.90	14.40	12.20	12.40	16.50	17.80	15.50	4.17	15.50	13.50	13.90	14.50	15.90	12.94	14.40	13.80	14.33
Fe_2O_3	0.77	1.37	1.50	1.71	1.52	1.55	0.63	0.42	3.08	3.00	2.02	0.24	1.84	1.26	1.31	1.72	1.69	1.33*	1.96	2.79*	2.2*
FeO	0.30	0.44	0.37	0.38	0.25	0.27	0.07	2.26	2.65	2.07	0.10	1.09	0.13	0.50	0.49	0.74	0.56		0.31		
MnO	0.02	0.04	0.03	0.08	0.06	0.02	0.02	0.03	0.57	0.03	0.09	0.03	0.05	0.06	0.08	0.10	0.06	0.12	0.05	0.12	0.05
MgO	0.21	0.49	0.40	0.58	0.35	0.36	0.10	0.16	5.19	1.73	0.12	7.59	0.18	0.40	0.45	0.68	1.88	0.14	0.60	0.73	0.62
CaO	0.82	1.08	1.03	0.95	0.61	0.78	0.33	0.38	4.81	3.82	0.70	10.50	0.54	1.11	0.82	1.41	0.96	0.25	1.90	1.56	1.44
Na_2O	3.78	4.01	4.16	4.43	3.88	4.16	3.99	3.57	4.78	5.23	8.81	1.32	3.99	3.82	4.00	4.65	5.25	4.46	3.64	3.95	4.02
K_2O	5.45	5.09	4.98	5.01	5.61	4.95	4.56	4.89	3.36	3.89	0.07	1.09	7.47	5.15	5.42	4.70	4.65	4.98	4.70	4.63	5.15
H_2O^+	0.32	0.35	0.33	0.80	0.40	0.44	0.16	0.40	1.42	0.49	0.34	0.95	0.32	0.24	0.19	0.36	0.52	0.38*	0.37	0.75*	0.81*
H_2O^-	0.33	0.38	0.10	0.56	0.24	0.09	0.06	0.15	0.37	0.12	0.35	0.57	0.18	0.23	0.10	0.26	0.37		0.24		
P_2O_5	0.08	0.10	0.10	0.19	0.08	0.13	0.05	0.05	0.74	0.52	0.08	0.11	0.07	0.10	0.20	0.17	0.58	0.08	0.09	0.09	0.15
CO_2	0.10	0.10	0.09	0.20	0.26	0.10	0.24	0.28	0.31	0.13	0.40	2.97	0.13	0.26	0.06	0.30	0.10		0.35		
Cl	0.12	0.06	0.13	0.04	0.03	0.03	0.02	0.03	0.02	0.05	0.01	0.02	0.01	0.02	0.02	0.04	0.02		0.01		
F	0.04	0.07	0.07	0.08	0.06	0.06	0.01	0.03	0.64	0.07	0.02	0.04	0.04	0.06	0.06	0.08	0.06		0.04		
Total	99.12	99.13	99.62	100.11	99.48	99.10	100.15	99.59	99.89	99.68	99.73	100.15	99.53	99.65	99.70	99.93	101.01	97.82	99.50	96.04	97.26
CIPW normative minerals																					
Q	28.2	25.6	26.0	22.4	26.3	26.4	36.3	32.4	0.0	5.7	17.8	33.8	15.7	29.2	26.9	22.6	16.8	29.4	28.1	26.4	24.7
C	0.2	0.3	0.3	1.0	0.5	1.1	0.2	0.7	0.0	0.0	0.0	0.0	0.0	0.6	0.7	0.5	2.2	0.0	1.0	0.0	0.0
OR	32.2	30.1	29.4	29.6	33.1	29.2	26.9	28.9	19.9	23.0	0.4	6.4	44.1	30.7	32.2	30.0	27.5	29.7	28.1	27.7	30.6
AB	32.0	33.9	35.2	37.5	32.8	35.2	33.8	30.2	40.4	44.3	74.5	11.2	33.8	32.4	33.9	39.3	44.2	38.1	31.1	33.8	3.0
AN	3.5	4.7	4.5	3.5	2.5	3.0	1.3	1.6	13.6	13.6	2.5	2.2	2.2	2.9	2.1	3.5	0.3	0.6	6.5	6.3	34.2
DI	0.0	0.0	0.0	0.0	0.0	0.0	0.0	0.0	4.2	1.5	0.0	38.4	0.0	0.0	0.0	0.0	0.0	0.0	0.0	0.1	0.0
HY (EN+FS)	0.5	1.2	1.0	1.4	0.9	0.9	0.2	4.0	6.1	3.8	0.3	2.0	0.4	1.0	1.1	1.7	4.7	0.4	1.5	1.8	1.6
MT	0.2	0.5	0.3	0.3	0.0	0.0	0.0	0.6	4.4	4.4	0.0	0.3	0.0	0.8	0.7	1.5	0.8	0.0	0.2	0.0	0.0
HM	0.6	1.0	1.3	1.5	1.5	1.6	0.6	0.0	4.5	0.0	2.0	0.0	1.8	0.7	0.8	0.7	1.2	1.3	1.9	2.8	2.2
IL	0.5	0.7	0.6	0.8	0.6	0.6	0.2	0.3	0.0	1.4	0.4	0.9	0.4	0.7	0.8	0.8	0.8	0.3	0.7	0.3	0.1
TN	0.0	0.0	0.0	0.0	0.0	0.0	0.0	0.0	2.2	0.0	0.3	0.0	0.0	0.0	0.0	0.0	0.0	0.1	0.0	0.6	0.2
RU	0.0	0.0	0.0	0.0	0.0	0.0	0.0	0.0	0.0	0.0	0.1	0.0	0.2	0.0	0.0	0.0	0.0	0.0	0.0	0.0	0.2
AP	0.2	0.2	0.2	0.4	0.2	0.3	0.1	0.1	0.0	1.2	0.2	0.3	0.2	0.2	0.5	0.4	1.4	0.2	0.2	0.2	0.4

Trace element geochemistry (ppm)																					
Nb	48	30	30	28	30	30	60	32	14	26	60	10	60	28	38	34	31	114	16	14	29
Rb	186	150	168	195	168	166	237	202	247	95	10	24	314	170	170	150	139		120	120	
Sr	206	237	219	312	155	210	8	56	867	967	28	46	88	160	166	290	231	17	290	229	240
Zr	260	250	280	310	260	300	150	116	230	380	510	150	520	270	275	330	301	322	200	188	163
Y	30	30	32	32	34	38	16	14	30	28	34	20	40	34	46	32	29	32	20	19	18
Ba	630	750	710	960	690	710	40	200	1250	1850	640	320	480	500	620	780	700	86	1050	809	1150
Cu	20	20	20	20	20	20	20	36	20	20	20	20	20	20	20	20		15	20		
Ni	20	20	20	20	20	20	20	26	98	20	20	20	20	20	20	20		21	20		12
Zn	26	60	40	80	48	50	20	32	250	45	60	30	54	64	46	90		78	56		32
U																				4	
Th																				17	
Rare earth element geochemistry (ppm)																					
La	37.60	44.00	60.50	71.80	58.50	65.10	39.10	36.00	82.30	81.40	140.00	6.00	124.00	65.20	70.00	71.00	91.00	56.38	46.00	44.10	41.49
Ce	87.90	91.90	124.00	134.00	122.00	119.00	59.10	46.00	151.00	156.00	270.00	18.00	240.00	132.00	130.00	130.00	160.00	102.56	76.00	69.60	69.53
Pr	11.10	10.20	13.30	15.60	13.50	14.10	4.40	4.90	18.30	17.30	26.00	2.80	25.70	15.00	13.00	14.00	17.00		7.40	8.40	
Nd	39.00	36.70	44.90	53.80	45.60	46.80	10.10	16.00	70.10	60.40	89.00	12.00	82.10	50.00	46.00	49.00	62.00	29.19	26.00	24.60	21.41
Sm	6.70	6.40	7.50	9.00	8.10	7.80	1.20	2.30	11.60	8.80	13.00	2.70	12.30	8.06	7.00	6.90	8.80	5.66	3.70	4.10	3.96
Eu	0.91	0.93	1.03	1.33	1.00	1.16	0.08	0.35	2.89	2.19	1.60	0.44	1.55	0.97	1.10	0.91	1.00	0.43	0.71	0.81	0.68
Gd	5.70	5.30	6.00	7.40	6.20	5.80	1.20	1.70	8.60	6.10	7.30	2.40	8.30	6.07	4.40	4.70	7.00	4.70	2.90	3.30	3.16
Tb	1.00	1.00	1.00	1.00	1.00	1.00	1.00	0.30	1.00	1.00	0.97	0.34	1.00	1.00	0.67	0.83	1.10		0.47	0.50	
Dy	4.90	4.60	5.00	5.80	4.40	4.40	0.50	1.60	5.30	3.90	5.80	2.20	6.40	5.50	4.30	4.60	5.90	4.29	2.40	2.90	2.69
Ho	0.97	0.90	0.95	1.08	0.99	0.80	0.19	0.36	0.97	0.66	1.20	0.42	1.21	1.03	0.90	0.87	1.10	0.82	0.52	0.59	0.66
Er	2.80	2.40	2.70	2.90	2.60	2.10	0.70	1.20	2.30	1.50	3.30	1.40	3.20	2.60	2.20	2.40	3.20		1.60	2.00	
Tm	0.46	0.40	0.42	0.47	0.43	0.30	0.14	0.18	0.36	0.24	0.49	0.20	0.53	0.40	0.35	0.35	0.52		0.25	0.40	
Yb	3.00	2.30	2.70	2.60	2.50	1.90	1.00	1.60	2.00	1.30	3.40	1.80	3.50	2.50	3.20	2.70	3.30	3.17	1.40	2.10	1.72
Lu	0.41	0.32	0.37	0.37	0.36	0.27	0.18	0.00	0.00	0.00	0.00	0.00	0.51	0.35				0.49		0.28	0.27

Note: Analytical methods described in Calzia (1990). Sample 126 was analyzed at the XRAL laboratories (Toronto) using methods described in Rämö et al. (2002).

* Total iron or total water.

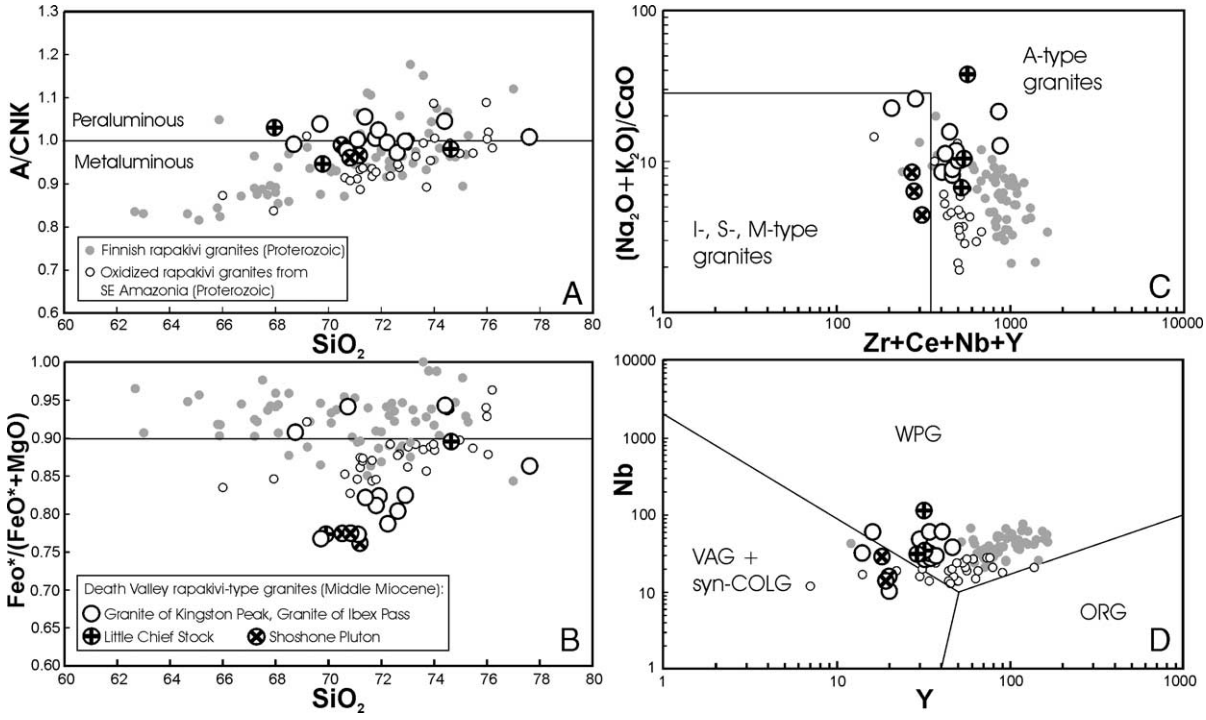

Fig. 4. Chemical composition of Miocene rapakivi granites from the southern Death Valley region compared with "type" 1.6-Ga Finnish rapakivi granites (Rämö and Haapala, 1995), and oxidized 1.88-Ga anorogenic granites from the southeastern flank of the Amazonian craton, Brazil (Dall'Agnol et al., 1999). (A) A/CNK vs SiO_2; (B) FeO*/(FeO*+MgO) vs SiO_2; (C) $(Na_2O+K_2O)/CaO$ vs Zr+Ce+Nb+Y; and (D) Nb vs Y diagrams. A/CNK=molecular $Al_2O_3/(CaO+Na_2O+K_2O)$, FeO*=total Fe expressed as FeO. Fields in (C) and (D) from Whalen et al. (1987) and Pearce et al. (1984), respectively: WPG—within plate granites, ORG—ocean ridge granites, VAG—volcanic arc granites, syn-COLG—syn-collision granites.

kivi granites are less influenced by upper crustal contamination (higher ε_{Nd}, lower Sr_i) than the Cretaceous plutons from Death Valley (Fig. 6; Rämö et al., 2002), but were probably derived from more evolved source rocks (lower ε_{Nd}, higher Sr_i) than most of the Peninsular Ranges and Sierra Nevada batholiths. These data indicate that the rapakivi granites in the southern Death Valley region include a juvenile or mantle component in their source rocks. In terms of Nd isotopes, the three plutons in the southern Death Valley region are similar, with initial ε_{Nd} values of about -6 to -7; this variation barely exceeds the experimental error of ε_{Nd}. In contrast, the initial Sr isotope composition shows more scatter (Sr_i=0.7059–0.7126) and could reflect contamination of the granitic magmas from source or country rocks with varying Sr isotope composition.

The Pb isotope composition of the Miocene rapakivi-type granites in the southern Death Valley region is shown in Fig. 7. The samples show relatively little variation and, in both diagrams, fall close to the boundary between the Precambrian Mojave and Arizona crustal provinces (MCP and ACP, respectively) of Wooden and Miller (1990). Pb isotopes of the rapakivi granites are also more radiogenic than those of Cretaceous batholiths of the southern Death Valley region. This is compatible with the hypothesis of a marked post-Cretaceous mantle component in the rapakivi granites of the southern Death Valley region.

5. Emplacement and crystallization history

Stratigraphic reconstruction of Proterozoic, Paleozoic, and Miocene country rocks in the Kingston Range as well as regional tectonic relations suggest that the granite of Kingston Peak was emplaced at shallow (≤4 km) crustal levels in an actively extend-

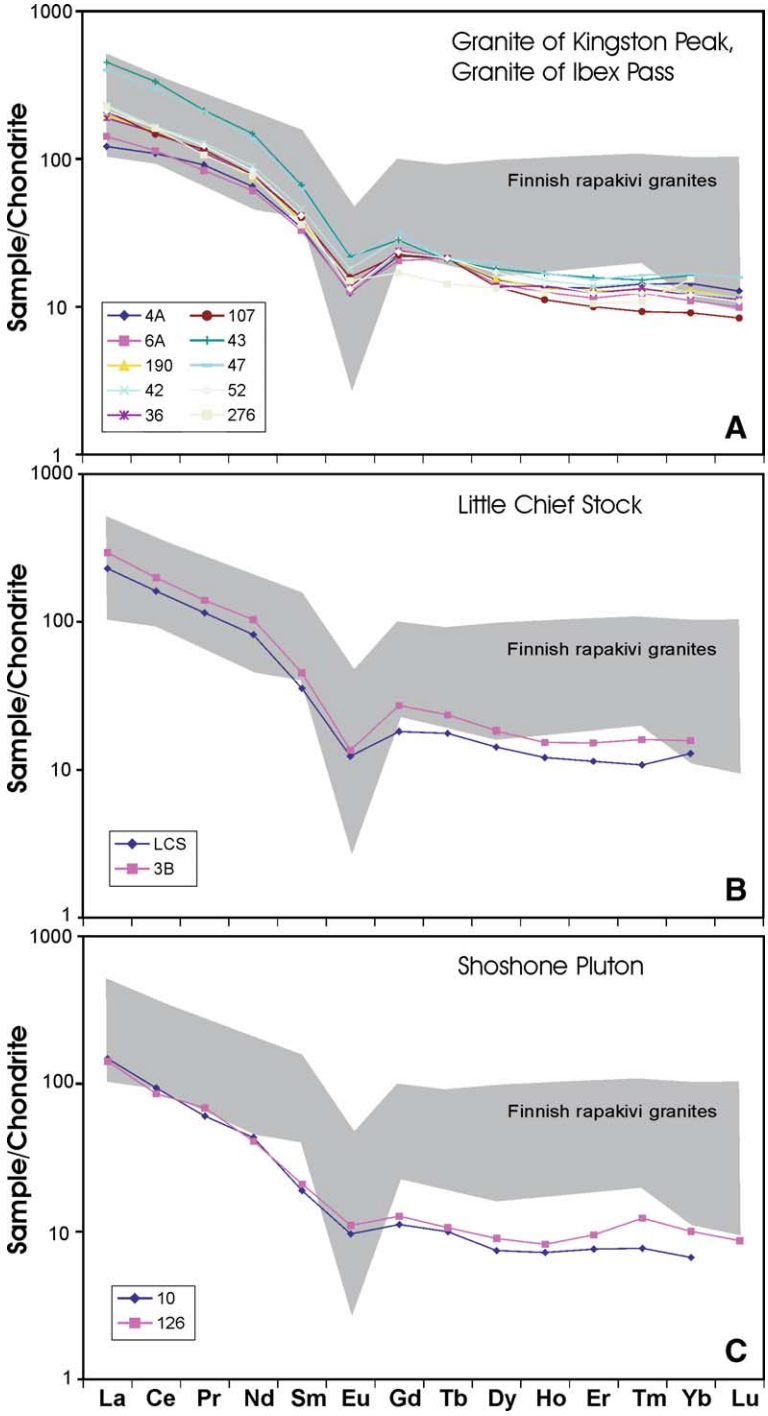

Fig. 5. Chondrite-normalized rare earth element patterns of rapakivi-type granite plutons from the southern Death Valley region: (A) Granite of Kingston Peak, Granite of Ibex Pass; (B) Little Chief stock; (C) Shoshone pluton. Overall field for the Finnish rapakivi granites (Haapala et al., 2005) is also shown.

Table 3
Isotopic data of Miocene rapakivi granites, southern Death Valley, California

Area	Kingston Range									Sperry Hills		Panamint Mtns	Greenwater Mtns	
Name	Granite of Kingston Peak (12.4 Ma)							Mafic xenolith	Syenite, Peak 4611	Granite of Ibex Pass		Little Chief stock (10.6 Ma)	Shoshone pluton (9.8 Ma)	
Description	Feldspar porphyry facies			Quartz porphyry facies			Aplite facies					Southern phase		
Sample no.	4A	6A	190	42	36	107	H3	173	47	52	7A	LCS	10	126
Lead isotopic data														
$^{206}Pb/^{204}Pb$	19.236	19.183	19.209	19.177	19.194	19.162	19.103	18.903	18.982	19.211	19.210	19.101	18.782	18.821
$^{207}Pb/^{204}Pb$	15.695	15.680	15.694	15.675	15.678	15.688	15.671	15.646	15.672	15.699	15.683	15.662	15.648	15.661
$^{208}Pb/^{204}Pb$	39.674	39.541	39.631	39.503	39.559	39.563	39.337	38.786	39.143	39.675	39.655	39.405	39.425	39.354
Strontium isotopic data														
Rb (ppm)	155	150	168	159	168	166	237	247	274	179	176	155	126	128
Sr (ppm)	182	237	219	274	155	210	8	867	77	156	143	288	291	238
Rb/Sr	0.852	0.633	0.767	0.580	1.080	0.790	29.620	0.285	3.580	1.150	1.230	0.538	0.433	0.538
$^{87}Rb/^{86}Sr$	2.470	1.830	2.220	1.670	3.140	2.290	85.760	0.825	10.370	3.320	3.560	1.560	1.250	1.550
$^{87}Sr/^{86}Sr$	0.7130	0.7088	0.7091	0.7090	0.7099	0.7091	0.7211	0.7075	0.7123	0.7102	0.7108	0.7081	0.7085	0.7082
Sr_i	0.7126	0.7085	0.7087	0.7087	0.7094	0.7087	0.7059	0.7074	0.7105	0.7096	0.7102	0.7079	0.7083	0.7080
Neodymium isotopic data														
Sm (ppm)	6.469		7.646		7.808	10.490	1.345	9.501	11.460			7.867		3.658
Nd (ppm)	37.40		46.26		45.14	63.55	10.84	62.72	78.45			48.93		23.05
$^{147}Sm/^{144}Nd$	0.10360		0.09994		0.10460	0.09977	0.07502	0.09157	0.08832			0.09720		0.09593
$^{143}Nd/^{144}Nd$	0.512236		0.512271		0.512270	0.512269	0.512340	0.512312	0.512345			0.512308		0.512308
$\varepsilon_{Nd\ i}$	−7.7		−7.0		−7.0	−7.0	−5.6	−6.2	−5.5			−6.3		−6.3
T_{DM} (Ma)	1118		1037		1081	1038	781	918	854			966		956

Note: for analytical methods used, see Wooden et al. (1988) for Pb and Sr isotopes, and Rämö et al. (2002) for Nd isotopes as well as Pb and Sr isotopes for sample 126. Sr and Nd initial compositions corrected for age (Miocene) of crystallization.

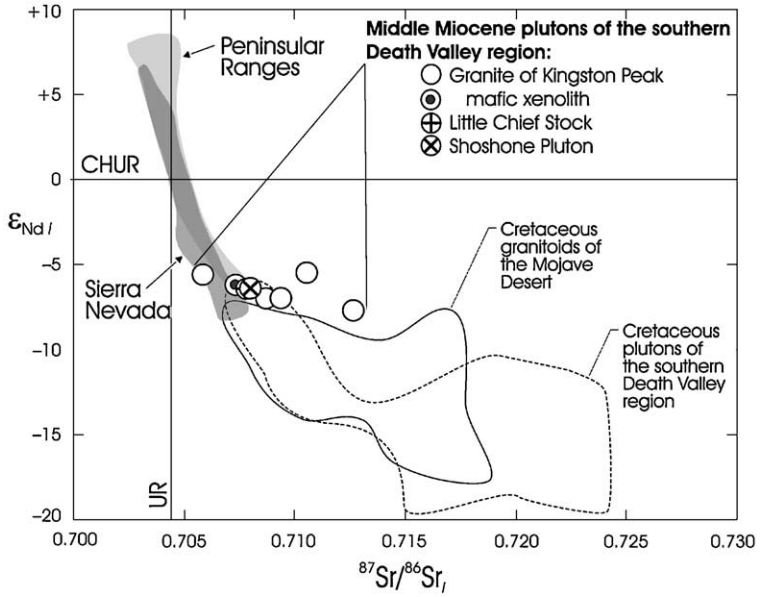

Fig. 6. Diagram comparing initial ε_{Nd} and $^{87}Sr/^{86}Sr$ values of Miocene rapakivi granites from the southern Death Valley region (this study) to Cretaceous granitoids in the southern Death Valley region, western and eastern Mojave Desert, and the Sierra Nevada and Peninsular Ranges batholiths (data from Kistler and Peterman, 1973, 1978; DePaolo, 1981; Kistler et al., 1986; Miller and Wooden, 1994; Allen et al., 1995; Barth et al., 1995, Gerber et al., 1995; Mahood et al., 1996; Rämö et al., 2002). CHUR is Chondritic Uniform Reservoir; UR is Sr uniform mantle reservoir (DePaolo and Wasserburg, 1976).

ing orogen (Calzia, 1990). The abundance of randomly oriented oligoclase inclusions near the cores of K-feldspar phenocrysts and K-feldspar inclusions near the cores of plagioclase phenocrysts indicate that plagioclase and K-feldspar began to crystallize early and at about the same time; the relative size and abundance of the phenocrysts suggest, however, that plagioclase was the liquidus phase. Quartz also occurs as randomly oriented inclusions or as blebs mantled by K-feldspar near the cores of the feldspar phenocrysts. The coexistence of quartz, K-feldspar, and(or) plagioclase inclusions suggests that the granitic melt quickly reached eutectic conditions early in its crystallization history. The abundance of biotite and hornblende in the groundmasses of the feldspar and quartz porphyry facies and as inclusions near the margins of the feldspar phenocrysts suggests that the mafic minerals began to crystallize after plagioclase, K-feldspar, and quartz.

Comparison of the interpreted crystallization sequence with experimental studies of granitic systems, combined with the abundances of titanite, magnetite, and quartz, suggest that the feldspar porphyry facies crystallized at 675 °C and at high oxygen fugacity (f_{O_2}>NNO but <HM buffer curves). Late crystallization of hydrous minerals indicates that the volatile content (primarily H_2O) varied from less than two weight percent near the liquidus to saturation near the solidus; the abundance of miarolitic cavities in the groundmass of all three facies indicates that a volatile phase was exsolved during late-stage crystallization of the granitic melt (Calzia, 1990).

Granitic magma that crystallized to form the Little Chief stock was probably injected into a narrow, vertical east-trending feeder dike, then expanded laterally and upward to form a laccolith-like plug along the contact between gneiss and the Pahrump Group (McDowell, 1967, 1974). Assuming that the magmatic inclusions were incorporated at this time, the feeder dike may have been located along the zone of inclusions near the contact between the southern and northern facies; this zone of inclusions coincides with a zone of faulting, breccia, and small plugs that are synmagmatic with the stock. Initial doming and extension of the country rocks caused formation of west-dipping normal faults north of the Little Chief stock

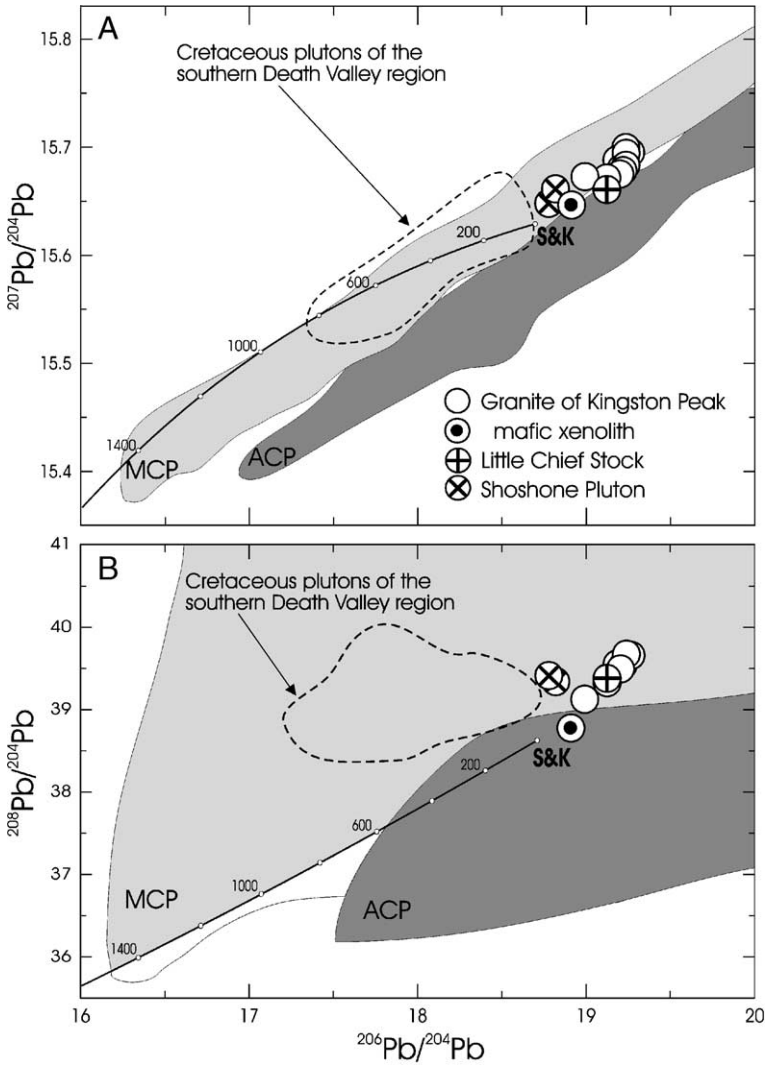

Fig. 7. Pb isotope composition of Miocene rapakivi granites from the southern Death Valley region. Fields for Cretaceous granitoids of the southern Death Valley region from Rämö et al. (2002); MCP and ACP represent Precambrian Mojave and Arizona crustal provinces, respectively (Wooden and Miller, 1990). S and K denotes the growth curves of average crustal Pb (Stacey and Kramers, 1975); numbers on the growth curves are model ages in Ma.

followed by intrusion of the northern dike swarm. Continued injection of magma resulted in formation of a trapdoor structure consisting of a nearly rectangular block of sedimentary country rocks bounded by vertical faults. As magma was injected, the western half of the trapdoor structure was tilted east; differential uplift of the trapdoor resulted in offset of the northern dike swarm along the trapdoor faults. McDowell concluded that the southern facies was at its present position during formation of the trapdoor structure; intrusion of the northern facies resulted in truncation and deformation of the northern dike swarm and produced sharply discordant contacts with the country rocks.

Petrographic data suggest that plagioclase, augite, and magnetite were the early liquidus phases of the Little Chief stock (McDowell, 1967, 1978). Plagioclase phenocrysts, however, are zoned from labradorite to andesine and oligoclase; many of these phenocrysts are partially resorbed and reversely

zoned. With continued crystallization, sanidine phenocrysts began to crystallize with oligoclase; augite became unstable and hornblende began to crystallize with biotite and magnetite. McDowell reported that these changes in phenocryst composition and stability were caused by progressive changes in water content and P_{H_2O} as the magma crystallized. With crystallization of feldspar and augite, water content and P_{H_2O} increased. Eventually P_{H_2O} exceeded P_{load}, and the magma moved up in the crust to a level where $P_{H_2O}=P_{load}$ and crystallization continued. During ascent, plagioclase phenocrysts were partially resorbed and zoned with more Na-rich compositions; with continued crystallization, a more Ca-rich plagioclase became the stable phase, resulting in reversals of zoned-plagioclase compositions. The process was repeated until both plagioclase and sanidine were stable. McDowell (1967) concluded that sanidine began to crystallize at 710–680 °C and 1.0–2.5 kbar; assuming a crustal density of 2.85 gm/cm^3, two feldspar crystallization probably began at a depth of 6–6.5 km.

Intrusion of the magma into the Pahrump Group resulted in assimilation of dolomitic or calcareous country rocks relatively rich in H_2O and CO_2 (McDowell, 1967, 1974). With a sudden increase in P_{fluid} (where $P_{fluid}=P_{H_2O}+P_{CO_2}$) or decrease in P_{load}, the feldspars become unstable. Sanidine phenocrysts reacted with the melt and were partially resorbed and rimmed by oligoclase, resulting in the formation of rapakivi textures; oligoclase rims may also have formed on plagioclase phenocrysts at this time. Assimilation of dolomitic country rocks also resulted in formation of diopside rims around hornblende; cumulophyric aggregates of plagioclase, biotite, and hornblende probably resulted from assimilation of calcareous greywacke from the upper Pahrump Group.

Episodic increase of water content followed by relatively rapid loss of P_{fluid} probably resulted in biotite pseudomorphs after hornblende as well as simultaneous crystallization of K-feldspar and quartz in the groundmass. Continued crystallization of the groundmass resulted in high volatile concentrations and formation of a vapor phase as indicated by the abundance of vugs, pegmatite dikes, and graphic-granite textures in the northeast part of the northern facies. With the bulk of the groundmass crystallized, biotite reacted with a vapor phase to form magnetite or hematite; magnetite reacted with the volatile-rich phase to form hematite. The appearance of these minerals indicates high oxygen fugacity during final crystallization. Based on this crystallization sequence, McDowell (1967) concluded that the Little Chief stock finally crystallized at 670–620 °C and 0.4–0.9 kbar.

The emplacement history of the Shoshone pluton is enigmatic. This pluton has no exposed intrusive contacts and is disconformably overlain by the volcanics of Deadman Pass and the Miocene Shoshone Volcanics. Fragments of the quartz monzonite are found in tuff of the Shoshone Volcanics at the contact; these relations show that the Shoshone pluton formed the erosional surface beneath the Miocene tuff.

The rim and core facies have similar whole-rock and feldspar compositions but different groundmass textures; the groundmass textures were controlled by water contents (Almashoor, 1980). The abundance of miarolitic cavities suggests that the rim facies contained more water than the core facies and crystallized more slowly, resulting in the coarser-grained granophyric groundmass. The abundance of biotite relative to hornblende suggests, however, that the rim facies initially contained less than three percent H_2O. With crystallization, the magma became saturated in water. Eventually $P_{H_2O}>P_{total}$, the wall rock was fractured, and magma intruded to higher crustal levels. This process was repeated until the magma was emplaced in a subvolcanic environment and crystallized rapidly, resulting in the aphanitic groundmass of the core facies. Almashoor estimated that the magma finally crystallized at a depth of 2.5–2.0 km (P is approximately 0.8–0.5 kbar). Assuming $P\leq 1.0$ kbar and using two-feldspar geothermometry, he concluded that the Shoshone pluton crystallized at 750–850 °C.

6. Concluding remarks

The Miocene rapakivi granites of the southern Death Valley region include the 12.4-Ma granite of Kingston Peak, the ca. 10.6-Ma Little Chief stock, and the 9.8-Ma Shoshone pluton; the granite of Ibex Pass is a landslide breccia of the granite of Kingston Peak. Textural variations and intrusive relations show that each of these plutons is zoned inward from a porphyritic rim facies to an equigranular aplite core; all

porphyritic facies are characterized by rapakivi texture and miarolitic cavities. Mafic xenoliths and inclusions are common; they probably represent earlier magmatic phases that were partially resorbed during crystallization. Regional stratigraphic and tectonic data indicate that all three plutons were emplaced at shallow crustal levels in an actively extending orogen.

Petrographic data suggest that each rapakivi granite in the southern Death Valley region evolved through a long and complex crystallization history of anhydrous magma. Crystallization of anhydrous minerals, primarily feldspars and pyroxenes, increased water content and P_{H_2O}. Eventually P_{H_2O} will exceed P_{load}, the country rock fractured, and the magma moved to a higher crustal level. Minor amounts of normative anorthite (cf. Table 3) are indicators of early crystallization of plagioclase and K-feldspar in equilibrium with melt along the cotectic between plagioclase and K-feldspar fields in the Q–Or–Ab–H_2O system (Tuttle and Bowen, 1958). A sudden loss of volatiles caused an abrupt decrease in pressure and shifted the cotectic toward the Or apex. The melt compensated for this shift by crystallizing plagioclase; K-feldspar was resorbed and did not crystallize until the composition of the melt reached the new cotectic. Plagioclase nucleated and crystallized either as new crystals or as mantles on existing feldspars. The overgrowth of plagioclase on partially resorbed K-feldspar crystals resulted in rapakivi texture.

Geochemical data show that the Miocene rapakivi granites in the southern Death Valley region straddle the peraluminous–metaluminous boundary and are more oxidized and less clearly A-type than rapakivi granites from Finland. Overall, the Pb and Sr isotope data are compatible with the idea that the rapakivi granites from Death Valley were derived by partial melting of Mesozoic plutonic rocks; Nd isotope data, however, suggest that all these three Miocene plutons include a juvenile (mantle) component. These data, combined with the volume of coeval volcanic rocks in the region (Fig. 2), suggest that heat required for melting may be transported into the crust by magmatic underplating. If so, then the Miocene rapakivi granites in the southern Death Valley region were generated by similar magmatic processes as Proterozoic rapakivi granites of southern Finland and the Amazonian craton. Although previous Sr isotope data suggest that the granite of Kingston Peak could have been derived by partial melting of Mesozoic plutonic rocks (Calzia, 1990), our new Sr, Nd, and Pb isotope data do not support this hypothesis. The Nd isotope composition suggests that all three plutons included a juvenile (mantle) component in their source area; Pb isotope data imply that the Pb in these rocks may have been derived from metamorphosed Early Proterozoic supracrustal rocks and granitoids of the Mojave crustal province. Seismic modeling implies that the lower crust beneath Death Valley consists of relatively low-velocity ductily deformed crustal material interlayered with and underplated by numerous relatively high-velocity subhorizontal mafic sills probably derived from the mantle (McCarthy and Thompson, 1988; Serpa et al., 1988). Combined, our isotope data and the seismic models suggest that rapakivi granites in the southern Death Valley region may be derived by partial melting of lower crustal rocks; the heat required for melting may be transported into the crust by magmatic underplating. Thus the Miocene rapakivi granites in the southern Death Valley region could have been generated by similar magmatic processes as Proterozoic rapakivi granites of southern Finland and the Amazonian craton.

Acknowledgments

The authors thank B.W. Troxel for providing field accommodations in Shoshone, CA, J.L. Wooden, USGS, for Pb and Sr analyses of selected samples, and the staff of Isotope Geology, Geological Survey of Finland, for help while performing the isotopic analyses. We also thank R.L. Christiansen and E.H. McKee, Jr., both from the USGS, for critical and thoughtful reviews of the manuscript. Rämö's research in the southern Death Valley region was funded by the Academy of Finland (Project SA 36002).

References

Albee, A.L., Labotks, T.C., Lanphere, M.A., McDowell, S.D., 1981. Geologic map of the Telescope Peak Quadrangle, California. U.S. Geological Survey Geologic Quadrangle Map 1532.

Almashoor, S.S., 1980. The petrology of a quartz monzonite pluton in the southern Greenwater Range, Inyo County, California. Ph.D. Thesis, Pennsylvania State University.

Allen, C.M., Wooden, J.L., Howard, K.A, Foster, D.A., Tosdal, R.M., 1995. Sources of the Early Cretaceous plutons in the Turtle and West Riverside Mountains, California: anomalous Cordilleran interior intrusions. Journal of Petrology 36, 1675–1700.

Amelin, Yu.V., Heaman, L.M., Verchogliad, V.M., Skobelev, V.M., 1994. Geochronological constraints on the emplacement history of an anorthosite–rapakivi granite suite: U–Pb zircon and baddeleyite study of the Korosten complex, Ukraine. Contributions to Mineralogy and Petrology 116, 411–419.

Amelin, Yu.V., Larin, A.M., Tucker, R.D., 1997. Chronology of multiphase emplacement of the Salmi rapakivi granite–anorthosite complex, Baltic Shield: implications for magmatic evolution. Contributions to Mineralogy and Petrology 127, 353–368.

Anderson, J.L., 1983. Proterozoic anorogenic granite plutonism of North America. In: Medaris Jr., L.G., Byers, C.W., Mickelson, D.M., Shanks, W.C. (Eds.), Proterozoic Geology: Selected Papers from an International Proterozoic Symposium, Geological Society of America, Memoir 161, 133–154.

Anderson, J.L., Bender, E.E., 1989. Nature and origin of Proterozoic A-type granitic magmatism in the southwestern United States of America. Lithos 23, 19–52.

Barth, A., Wooden, J.L., Tosdal, R.M., Morrison, J., 1995. Crustal contamination in the petrogenesis of a calc-alkalic rock series: Josephine Mountain intrusion, California. Geological Society of America Bulletin 107, 201–212.

Burchfiel, B.C., Walker, J.D., Davis, G.A., 1983. Kingston Range and related detachment faults — a major "breakaway" zone in the southern Great Basin. Abstracts with Programs—Geological Society of America 15, 536.

Burchfiel, B.C., et al., 1985. The Kingston Range detachment system: structures at the eastern edge of the Death Valley extensional zone, southeastern California. Abstracts with Programs—Geological Society of America 17, 345.

Calzia, J.P., 1990. Geologic studies in the Kingston Range, southern Death Valley region, California. Ph.D. Thesis, University of California, Davis.

Calzia, J.P., Finnerty, A.A., 1984. Geologic and geochemical reconnaissance of Late Tertiary granitic plutons, Death Valley, California. Abstracts with Program—Geological Society of America 16, 461.

Calzia, J.P., Rämö, O.T., 2000. Late Cenozoic crustal extension and magmatism. Southern Death Valley region, California. In: Lagerson, D.R., Peters, S.G., Lahren, M.M. (Eds.), Great Basin and Sierra Nevada, Field Guide—Geological Society of America 2, 135–164.

Calzia, J.P., Verosub, K.L., Jachens, R.C., 1986. Tilting and faulting of the late Miocene Kingston Peak granite, southern Death Valley, California. EOS 67, 1189.

Calzia, J.P., Blakely, R.J., Jachens, R.C., 1991. Miocene magmatism and extension in Ibex Pass, southern Death Valley, California. EOS 72, 469.

Cemen, I., Wright, L.A., Prave, A.R., 1999. Stratigraphy and tectonic implications of the latest Oligocene and early Miocene sedimentary succession, southwesternmost Funeral Mountains, Death Valley region, California. In: Wright, L.A., Troxel, B.W. (Eds.), Cenozoic Basins of the Death Valley Region, Special Paper—Geological Society of America 333, 65–86.

Dall'Agnol, R., Rämö, O.T., de Magalhães, M.S., Macambira, M.J.B., 1999. Petrology of the anorogenic, oxidized Jamon and Musa granites, Amazonian Craton: implications for the genesis of Proterozoic A-type granites. Lithos 46, 431–462.

DePaolo, D.J., 1981. A neodymium and strontium isotopic study of the Mesozoic calc-alkaline granitic batholiths of the Sierra Nevada and Peninsular Ranges, California. Journal of Geophysical Research 86, 10470–10488.

DePaolo, D.J., Wasserburg, G.J., 1976. Nd isotopic variations and petrogenetic models. Geophysical Research Letters 3, 249–252.

Dohrenwend, J.C., McFadden, L.D., Turrin, B.D., Wells, S.G., 1984. K–Ar dating of the Cima volcanic field, eastern Mojave Desert, California: Late Cenozoic volcanic history and landscape evolution. Geology 12, 163–167.

Eklund, O., Fröjdö, S., Lindberg, B., 1994. Magma mixing, the petrogenetic link between anorthositic suites and rapakivi granites, Åland, SW Finland. Contributions to Mineralogy and Petrology 50, 3–19.

Emslie, R.F., 1978. Anorthosite massifs, rapakivi granites, and late Proterozoic rifting of North America. Precambrian Research 7, 61–98.

Emslie, R.F., 1991. Granitoids of rapakivi granite — anorthosite and related associations. In: Haapala, I., Condie, K.C. (Eds.), Precambrian Granitoids — Petrogenesis, Geochemistry and Metallogeny, Precambrian Research 51, 173–192.

Falkner, C.M., Miller, C.F., Wooden, J.L., Heizler, M.T., 1995. Petrogenesis and tectonic significance of the calc-alkaline, bimodal Aztec Wash pluton, Eldorado Mountains, Colorado River extensional corridor. Journal of Geophysical Research 100, 10453–10476.

Fowler, T.K., Calzia, J.P., 1999. Kingston range detachment fault, southeastern Death Valley region, California: relation to Tertiary deposits and reconstruction of initial dip. In: Wright, L.A., Troxel, B.W. (Eds.), Cenozoic Basins of the Death Valley Region, Special Paper—Geological Society of America 333, 245–257.

Fowler, T.K., Friedmann, S.J., Davis, G.A., Bishop, K.M., 1995. Two-phase evolution of the Shadow Valley basin, southeastern California: a possible record of footwall uplift during extensional detachment faulting. Basin Research 7, 165–179.

Friedmann, S.J., 1996. Miocene strata below the Shadow Valley basin fill, eastern Mojave Desert, California. In: Reynolds, R.E., Reynolds, J. (Eds.), Punctuated Chaos in the Northeastern Mojave Desert, San Bernardino County Museum Association Quarterly 43, 123–126.

Friedmann, S.J., Davis, G.A., Fowler, T.K., 1996. Geometry, paleodrainage, and geologic rates from the Miocene Shadow Valley supradetachment basin, eastern Mojave Desert, California. In: Beratan, K.K. (Ed.), Reconstructing the History of Basin and Range Extension Using Sedimentology and Stratigraphy, Special Paper—Geological Society of America 303, 85–105.

Frost, C.D., Frost, B.R., 1997. Reduced rapakivi-type granites: the tholeiitic connection. Geology 25, 647–650.

Frost, C.D., Bell, J.M., Frost, B.R., Chamberlain, K.R., 2001. Crustal growth by magmatic underplating: isotopic evidence from the northern Sherman batholith. Geology 29, 515–518.

Gerber, M.E., Miller, C.F., Wooden, J.L., 1995. Plutonism at the interior margin of the Jurassic magmatic arc, Mojave Desert, California. In: Miller, D.M., Busby, C. (Eds.), Jurassic Magmatism and Tectonics of the North American Cordillera, Special Paper—Geological Society of America 299, 351–374.

Haapala, I., 1985. Metallogeny of the Proterozoic rapakivi granites of Finland. In: Taylor, R., Strong, D.F. (Eds.), Granite-Related Mineral Deposits. Canadian Institute of Mining and Metallurgy, pp. 123–131.

Haapala, I., Rämö, O.T., 1990. Petrogenesis of the rapakivi granites of Finland. In: Stein, H.J., Hannah, J.L. (Eds.), Ore-Bearing Granite Systems: Petrogenesis and Mineralizing Processes, Special Paper—Geological Society of America 246, 275–286.

Haapala, I., Rämö, O.T., 1999. Rapakivi granites and related rocks: an introduction. Precambrian Research 95, 1–7.

Haapala, I., Rämö, O.T., Frindt, S., 2005. Comparison of Proterozoic and Phanerozoic rift-related basaltic–granitic magmatism. In: Rämö, O.T. (Ed.), Granitic Systems—Ilmari Haapala Special Issue, Lithos 80, 1–32.

Heaman, L.M., Grotzinger, J., 1992. 1.08 Ga diabase sills in the Pahrump group, California: implications for the development of the Cordilleran miogeocline. Geology 20, 637–640.

Hewett, D.F., 1940. New formation names to be used in the Kingston Range, Ivanpah Quadrangle, California. Journal of the Washington Academy of Sciences 30, 239–240.

Hodges, K., McKenna, L.W., Harding, M.B., 1990. Structural unroofing of the central Panamint Mountains, Death Valley region, southeastern California. In: Wernicke, B.P. (Ed.), Basin and Range Extensional Tectonics at the Latitude of Las Vegas, Nevada, Special Paper—Geological Society of America 176, 377–390.

Holm, D.K., Snow, J.K., Lux, D.R., 1992. Thermal and barometric constraints on the intrusive and unroofing history of the Black Mountains: implications for timing, initial dip, and kinematics of detachment faulting in the Death Valley region, California. Tectonics 11, 507–522.

Holm, D.K., Pavlis, T.L., Topping, D.J., 1994. Black Mountains crustal section, Death Valley region, California. In: McGill, S.F., Ross, T.M. (Eds.), Geological Investigations of an Active Margin. Cordilleran Section Guidebook—Geological Society of America, pp. 31–54.

Kistler, R.W., Peterman, Z.E., 1973. Variations in Sr, Rb, K, Na, and initial Sr^{87}/Sr^{86} in Mesozoic granitic rocks and intruded wall rocks in Central California. Geological Society of America Bulletin 84, 3489–3512.

Kistler, R.W., Peterman, Z.E., 1978. Reconstruction of crustal blocks of California on the basis of initial strontium isotopic compositions of Mesozoic granitic rocks. U.S. Geological Survey Professional Paper 1071.

Kistler, R.W., Chappell, B.W., Peck, D.L., Bateman, P.C., 1986. Isotopic variation in the Tuolumne Intrusive Suite, central Sierra Nevada, California. Contributions to Mineralogy and Petrology 94, 205–220.

Lanphere, M.A., Wasserburg, G.J.F., Albee, A.L., Tilton, G.R., 1964. Redistribution of strontium and rubidium isotopes during metamorphism, World Beater Complex, Panamint Range, California. In: Craig, H., Miller, S.L., Wasserburg, G.J.F. (Eds.), Isotopic and Cosmic Chemistry. North Holland Publishing Company, Amsterdam, pp. 269–320.

Louie, J., et al., 1992. 7 Ma age of Tecopa Lake and tectonic quiescence from seismic stratigraphy east of Death Valley, California. EOS 73, 548.

Mahood, G.A., Nibler, G.E., Halliday, A.N., 1996. Zoning patterns and petrologic processes in peraluminous magma chambers: Hall Canyon pluton, Panamint Mountains, California. Geological Society of America Bulletin 108, 437–453.

McCarthy, J., Thompson, G.A., 1988. Seismic imaging of extended crust with emphasis on the western United States. Geological Society of America Bulletin 100, 1361–1374.

McDowell, S.D., 1967. The intrusive history of the Little Chief granite porphyry stock, Panamint Range, California. Ph.D. Thesis, California Institute of Technology.

McDowell, S.D., 1974. Emplacement of the Little Chief stock, Panamint Range, California. Geological Society of America Bulletin 85, 1535–1546.

McDowell, S.D., 1978. Little Chief granite porphyry: feldspar crystallization history. Geological Society of America Bulletin 89, 33–49.

McMackin, M.R., 1997. Late Tertiary evolution of the southern Death Valley fault system: the origin of the Tecopa hump, a tectonic dam on the Amargosa River. In: Reynolds, R.E., Reynolds, J. (Eds.), Death Valley: The Amargosa Route, San Bernardino County Museum Association Quarterly 44, 37–42.

Miller, C.F., Wooden, J.L., 1994. Anatexis, hybridization, and the modification of ancient crust: Mesozoic plutonism in the Old Woman Mountains area, California. Lithos 32, 111–133.

Neymark, L.A., Amelin, Yu., Larin, A.M., 1994. Pb–Nd–Sr isotopic constraints on the origin of the 1.54–1.56 Ga Salmi rapakivi granite–anorthosite batholith (Karelia, Russia). In: Haapala, I., Rämö, O.T. (Eds.), IGCP Project 315 Publication 12, pp. 173–194.

Pearce, J.A., Harris, N.B.W., Tindle, A.G., 1984. Trace element discrimination diagrams for the tectonic interpretation of granitic rocks. Journal of Petrology 25, 956–983.

Rämö, O.T., 1991. Petrogenesis of the Proterozoic rapakivi granites and related basic rocks of southeastern Fennoscandia: Nd and Pb isotopic and general geochemical constraints. Geological Survey of Finland, Bulletin 355.

Rämö, O.T., Calzia, J.P., 1998. Nd isotopic composition of cratonic rocks in the southern Death Valley region: evidence for a substantial Archean source component in Mojavia. Geology 26, 891–894.

Rämö, O.T., Haapala, I., 1995. One hundred years of rapakivi granite. Mineralogy and Petrology 52, 129–185.

Rämö, O.T., Calzia, J.P., Kosunen, J., 2002. Geochemistry of Mesozoic plutons, southern Death Valley region, California: insights into the origin of Cordilleran interior magmatism. Contributions to Mineralogy and Petrology 143, 416–437.

Salonsaari, P.T., 1995. Hybridization in the bimodal Jaala–Iitti complex and its petrogenetic relationship to rapakivi granites and associated mafic rocks of southeastern Finland. Geological Society of Finland, Bulletin 67.

Sederholm, J.J. 1891. Ueber die finnländischen Rapakiwigesteine: Tshermak's Mineralogische und Petrographische Mitteilungen 12, 1–31.

Serpa, L., deVoogd, B., Wright, L., Willemin, J., Oliver, J., Hauser, E., Troxel, B., 1988. Structure of the central Death Valley pull-apart basin and vicinity from COCORP profiles in the southern Great Basin. Geological Society of America Bulletin 100, 1437–1450.

Stacey, J.S., Kramers, J.D., 1975. Approximation of terrestrial lead isotope evolution by a two-stage model. Earth and Planetary Science Letters 26, 207–221.

Stern, T.W., Newell, M.F., Hunt, C.B., 1966. Uranium–lead and potassium–argon ages of parts of the Amargosa thrust complex, Death Valley, California. U.S. Geological Survey Professional Paper 550-B, 142–147.

Streckeisen, Albert, chairman, 1973. Plutonic rocks: classification and nomenclature recommended by the IUGS subcommission on the systematics of igneous rocks. Geotimes 18, 26–30.

Topping, D.J., 1993. Paleographic reconstruction of the Death Valley extended region: evidence from Miocene large rock–avalanche deposits in the Amargosa chaos basin, California. Geological Society of America Bulletin 105, 1190–1213.

Turrin, B.D., Dohrenwend, J.C., Drake, R.E., Curtis, G.H., 1985. K–Ar ages from the Cima volcanic field, eastern Mojave Desert, California. Isochron–West 44, 9–16.

Tuttle, O.F., Bowen, N.L., 1958. Origin of granite in the light of experimental studies in the system $NaAlSi_3O_8$–$KalSi_3O_8$–SiO_2–H_2O. Geological Society of America, Memoir 74 (153 pp.).

Volborth, A., 1973. Geology of the granite complex of the El dorado, Newberry, and northern Dead Mountains, Clark County, Nevada. Nevada Bureau of Mines and Geology, Bulletin 80, 40.

Whalen, J.B., Currie, K.L., Chappell, B.W., 1987. A-type granites: geochemical characteristics, discrimination, and petrogenesis. Contributions to Mineralogy and Petrology 95, 407–419.

Wernicke, B., Wlaker, J.D., Hodges, K., 1988. Field guide to the northern part of the Tucki Mountain fault system, Death Valley region, California. In: Weide, D.L., Faber, M.L. (Eds.), This Extended Land. Cordilleran Section Field Trip Guidebook—Geological Society of America, pp. 58–63.

Wooden, J.L., Miller, D.M., 1990. Chronologic and isotopic framework for Early Proterozoic crustal evolution in the eastern Mojave Desert region, SE California. Journal of Geophysical Research 95, 20133–20146.

Wooden, J.L., Stacey, J.S., Howard, K.A., 1988. Pb isotopic evidence for the formation of Proterozoic crust in the southwestern United States. In: Ernst, W.G. (Ed.), Metamorphism and crustal evolution, western conterminous United States, Prentice-Hall Ruby, vol. 7, pp. 68–86.

Wright, L.A., 1968. Talc deposits of the southern Death Valley–Kingston Range region, California. Special Report—California Division of Mines and Geology 95, 79.

Wright, L.A., Thompson, R.A., Troxel, B.W., Pavlis, T.L., DeWitt, E.H., Otton, J.K., Ellis, M.A., Miller, M.G., Serpa, L.F., 1991. Cenozoic magmatic and tectonic evolution of the east–central Death Valley region, California. In: Walawender, M.J., Hanan, B.B. (Eds.), Geological Excursions in Southern California and Mexico. Cordilleran Section Field Trip Guidebook—Geological Society of America, pp. 93–127.